Symmetric Box-splines on the $\mathcal{A}_n^*$ Lattice

Minho Kim

School of Computer Science,
University of Seoul,
Siripdae-gil 13, Dongdaemun-gu, Seoul, 130-743, Korea

Jörg Peters

Dept. of CISE,
University of Florida,
CSE Bldg., University of Florida, Gainesville, FL, 32611, USA

Abstract

Sampling and reconstruction of generic multivariate functions is more efficient on non-Cartesian root lattices, such as the BCC (Body-Centered Cubic) lattice, than on the Cartesian lattice. We introduce a new $n \times n$ generator matrix $\mathbf{A}^*$ that enables, in n variables, for efficient reconstruction on the non-Cartesian root lattice $\mathcal{A}_n^*$ by a symmetric box-spline family M_r^*. $\mathcal{A}_2^*$ is the hexagonal lattice and $\mathcal{A}_3^*$ is the BCC lattice. We point out the similarities and differences of M_r^* to the popular Cartesian-shifted box-spline family M_r, document the main properties of M_r^* and the partition induced by its knot planes and construct, in n variables, the optimal quasi-interpolant of M_2^*.

1. Introduction

Box-splines shifted on the *Cartesian lattice* are a useful generalization of uniform B-splines to several variables. In particular, a family M_r of n-variate box-splines is justly popular due to their linear independence and approximation properties (Section 3.3). Members of M_r are defined by r-fold convolution, in the n directions of the Cartesian grid plus a diagonal, so that the footprint of these box-splines is asymmetrically distorted in the diagonal direction. To make reconstruction of vector fields less biased, convolution and shifts on 2- and 3-dimensional non-Cartesian lattices have recently been advocated [33, 16, 17, 18, 15, 24]. For example, Kim *et al.* [24] show that reconstruction by a trivariate 6-direction C^1 box-spline of data on the FCC (Face-Centered Cubic) lattice both is more time-efficient by 35% and results in less aliasing of level sets than the standard C^1 tri-quadratic B-spline for the same number of samples on the Cartesian grid. Entezari *et al.* [16] show that the quality of reconstruction of the C^2 tri-cubic B-spline on the Cartesian grid is matched by reconstruction on the BCC lattice with the 8-direction C^2 box-spline, but using only 70% of data. In both cases, concrete implementations have established a computational speed advantage corresponding to the reduction of the number of convolution directions over the tensor-product B-spline of the same smoothness and approximation order.

In this paper, we generalize the bivariate box-splines on the hexagonal lattice and the trivariate box-splines on the BCC lattice to symmetric n-variate box-splines M_r^* (Section 5.3) defined by convolving along the

Email addresses: `minhokim@uos.ac.kr` (Minho Kim), `jorg@cise.ufl.edu` (Jörg Peters)

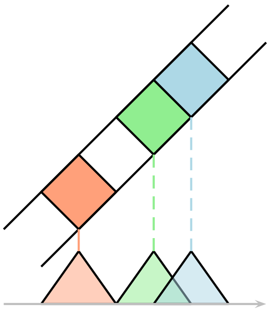

(a) $n = 1$

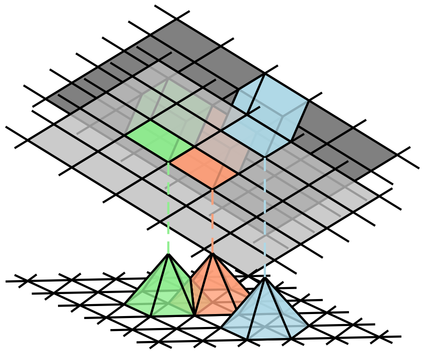

(b) $n = 2$

Figure 1: Orthogonal projection of a slab of unit cubes along the diagonal direction for (a) $n = 1$ and (b) $n = 2$.

nearest neighbor directions of the $\mathcal{A}_n^*$ *lattice* (Section 3.2). The $\mathcal{A}_n^*$ lattice is well-known in crystallography and discrete geometry. There it occurs (and is therefore defined as) a lattice embedded in an n-dimensional hyperplane of $\mathbb{R}^{n+1}$. By contrast to this standard formulation, we re-define the $\mathcal{A}_n^*$ lattice directly in $\mathbb{R}^n$ by introducing a new $n \times n$ generator matrix $\mathbf{A}^*$. Then the geometric construction of the shifts of the symmetric linear box-spline M_1^* on the $\mathcal{A}_n^*$ lattice simplifies to the classical construction of n-variate box-splines by projection: The shifts of the symmetric linear box-spline on $\mathcal{A}_n^*$ are the *orthogonal* projection of a slab of thickness 1 decomposed into unit cubes along the diagonal of the cubes (Figure 1). By comparison, M_1 (see Section 3.3) has the same preimage, but for $n \geq 2$, its support is distorted by its anisotropic direction matrix (Figure 7 (d)). Nevertheless, we can take full advantage of the close relationship of M_1^* and M_1 to analyze M_1^*. That is, this paper can apply existing mathematical machinery (non-trivially) in the service of bringing together ideas from signal processing and spline theory to show that the best reconstruction lattices have an associated symmetric box-spline family, *provided* that the newly derived matrix $\mathbf{A}^*$ is used to generate $\mathcal{A}_n^*$.

Specifically, this paper documents in *any* number of variables n, the support, its partition, the desirable properties shared with M_r and, for the important case $r = 2$, the quasi-interpolant construction associated with M_2^*. The four theorems of the paper summarize these results: Theorem 1 introduces the new square generator matrix $\mathbf{A}^*$, Theorem 2 lists the properties of M_r^*, Theorem 3 describes the support and partition induced by M_r^*, and Theorem 4 presents the optimal quasi-interpolant of M_2^*.

Overview of the paper. The paper combines ideas from signal processing and spline theory. So, after a review of related work in Section 2, we recall the pertinent facts of both areas used in the later proofs. Section 3 consists of subsection 3.1: lattice packing and optimal sampling, 3.2: the root lattices $\mathcal{A}_n$ and $\mathcal{A}_n^*$ and their standard geometric construction as subsets of $\mathbb{R}^{n+1}$, 3.3: the box-splines M_r. Readers conversant with optimal sampling lattices and box splines (in the notation of de Boor *et al.* [13]) might skip Section 3 after taking a look at our symbol glossary at its beginning. Sections 4 and 5 prepare for the main Section 6. Section 4 relates box-splines on non-Cartesian lattices to box splines on the Cartesian grid and shows how quasi-interpolation can be inherited by change-of-variables. Section 5 shows that the lattice $\mathcal{A}_n^*$ allows for a *symmetric* box-spline family M_r^* when represented in the form $\mathbf{A}^*\mathbb{Z}^n$ where $\mathbf{A}^*$ is a square generator matrix (Section 5.2) different from the standard geometric construction of $\mathcal{A}_n^*$ embedded in $\mathbb{R}^{n+1}$. Section 6 then documents the properties of the symmetric box-spline family M_r^* on $\mathcal{A}_n^*$.

2. Related Work

Piecewise linear *hat functions*, in particular the shifts of the bivariate 3-direction linear box-spline and of the trivariate 4-direction linear box-splines are popular basis functions for the 2D and 3D Finite Element Method, respectively. Linear hat functions apply to general triangular or tetrahedral meshes, but higher-degree box-splines, obtained by convolution along the mesh directions, require structured meshes. For a small sample of the literature on the bivariate 3-direction box-spline see [11, 12, 23, 7, 22, 2]. Chui and Lai [8] and Lai [26] derived efficient evaluation of convolutions of hat functions via the BB(Bernstein-Bézier)-form. Casciola *et al.* [4] extended this approach to three variables. Chang *et al.* [5, 6] proposed a volumetric subdivision scheme based on the trivariate 8-direction box-spline, M_2.

On the n-dimensional Cartesian grid, Arge and Dæhlen [1] investigated interpolation by M_r, and Shi and Wang [31] discussed the associated spline space. The literature refers to the space decomposition corresponding to the polynomial pieces of M_r as $(n+1)$-*directional mesh.*

The root lattices $\mathcal{A}_n$ and $\mathcal{A}_n^*$ are well-known in crystallography, discrete geometry and related areas. Conway and Sloane [9] provide a standard treatise of the subject. Here the lattices are embedded in $\mathbb{R}^{n+1}$ (Section 3.2). Hamitouche *et al.* [21] recognized the need for square generator matrices that embed the $\mathcal{A}_n$ and $\mathcal{A}_n^*$ lattices in $\mathbb{R}^n$. Their definition, in iterative bottom-up fashion, is however unnecessarily more complex and the resulting matrices are more complicated than the ones we will present in Section 5.2.

Frederickson [19] first discussed the (symmetric) bivariate splines on the hexagonal lattice. The hexagonal lattice is known to be the optimal sampling lattice in two dimensions and is equivalent to the $\mathcal{A}_2^*$ lattice. Van De Ville *et al.* [33] proposed *hex-splines* on the hexagonal lattice which share many properties with the box-splines on the hexagonal lattice. Similarly, the BCC lattice is the optimal 3D sampling lattice for functions with isotropic and band-limited frequencies [17, 15] and is equivalent to the $\mathcal{A}_3^*$ lattice [9]. Entezari *et al.* [16, 17, 18] and Entezari [15] were the first to investigate the (symmetric) trivariate 4- and 8-direction box-splines on the BCC lattice.

3. Notation and Background

The dimension of vectors and matrices is either explicitly given or is determined by context. Some of the specific vectors and matrices are:

- $\mathbf{i}_k$ the k-th unit vector,
- $\mathbf{I}_n$ the $n \times n$ identity matrix,
- $\mathbf{0} := \begin{bmatrix} 0 & \cdots & 0 \end{bmatrix}^t$ the zero vector,
- $\mathbf{j} := \begin{bmatrix} 1 & \cdots & 1 \end{bmatrix}^t$ the 'diagonal vector',
- $H_{\mathbf{j}}^n$ the n-dimensional hyperplane, embedded in $\mathbb{R}^{n+1}$, including $\mathbf{0}$ and with normal $\mathbf{j}$,
- $\mathbf{J}_n := \mathbf{j}\mathbf{j}^t$ the $n \times n$ matrix composed of 1s only.

The dot product is defined as $\boldsymbol{x} \cdot \boldsymbol{y} := \boldsymbol{x}^t \boldsymbol{y} \in \mathbb{R}$.

- Following the convention of de Boor *et al.* [13], an $n \times m$ matrix will be interpreted both as
  - a multi-set (bag) of column vectors or
  - a linear transformation $\mathbb{R}^m \to \mathbb{R}^n$.
- For the matrices $\boldsymbol{\Xi}$ and $\mathbf{Z}$, $\quad \boldsymbol{\Xi} \backslash \mathbf{Z} := \{\boldsymbol{\zeta} : \boldsymbol{\zeta} \in \boldsymbol{\Xi} \text{ and } \boldsymbol{\zeta} \notin \mathbf{Z}\}$.
- Column vectors are used as either vectors or points depending on the context.

- Linear *transformations*, e.g., $\mathbf{P}_n$ (Section 3.2), box-spline *matrices of directions* (Section 3.3), e.g., $\mathbf{\Xi}$ and $\mathbf{T}_r$, and lattice *generator matrices* (Section 3.1), such as $\mathbf{G}$, $\mathbf{A}_{\mathrm{P}}^*$ and $\mathbf{A}$, are typeset in upper bold.
- Lattices are typeset in calligraphic upper case; e.g., $\mathcal{L}_n$ and $\mathcal{A}_n$.
- $\boldsymbol{v}(j)$ denotes the j-th entry of the vector $\boldsymbol{v}$.
- $\mathbf{X}(i,j)$ denotes the (i,j)-th entry of the matrix $\mathbf{X}$.
- $\mathrm{conv}(P)$ is the *convex hull* of the points in P.

A matrix $\mathbf{B} \in \mathbb{Z}^{n\times m}$, $n \leq m$, is *unimodular* [13, (II.57)] if

$$\det \mathbf{Z} = \pm 1, \quad \forall \mathbf{Z} \subseteq \mathbf{B} : \mathbf{Z} \text{ is square and } \mathrm{rank}\mathbf{Z} = n.$$

If $n = m$ and $\mathbf{B} \in \mathbb{Z}^{n\times n}$ is unimodular then $\mathbf{B}^{-1} \in \mathbb{Z}^{n\times n}$.

3.1. Lattice packing and optimal sampling

A lattice is a discrete subgroup of maximal rank in a Euclidean vector space [28]. Given an $m \times n$ matrix $\mathbf{G}$ with $m \geq n$ and $\mathrm{rank}\mathbf{G} = n$, all integer linear combinations of its columns, $\mathbf{G}\mathbb{Z}^n$, define (the points of) an n-dimensional *lattice*, say $\mathcal{L}_n$, embedded in $\mathbb{R}^m$:

$$\mathcal{L}_n := \{\mathbf{G}\boldsymbol{j} \in \mathbb{R}^m : \boldsymbol{j} \in \mathbb{Z}^n\}.$$

$\mathbf{G}$ is called a *generator matrix* of $\mathcal{L}_n$, and we call the columns of $\mathbf{G}$ a *basis* of $\mathcal{L}_n$. The choice of a generator matrix for a lattice is not unique [28].

Lemma 1. *If* $\mathbf{U} \in \mathbb{Z}^{n\times n}$ *is* unimodular *then* $\mathbf{G}$ *and* $\mathbf{GU}$ *generate the same lattice points:* $\mathbf{G}\mathbb{Z}^n = \mathbf{GU}\mathbb{Z}^n$.

Proof. Since $\mathbf{U}\mathbb{Z}^n \subseteq \mathbb{Z}^n$, $\mathbf{G}(\mathbf{U}\mathbb{Z}^n) \subseteq \mathbf{G}\mathbb{Z}^n$. Conversely, $\mathbf{G}\mathbb{Z}^n = (\mathbf{GU})(\mathbf{U}^{-1}\mathbb{Z}^n) \subseteq \mathbf{GU}\mathbb{Z}^n$ since $\mathbf{U}^{-1}\mathbb{Z}^n \subseteq \mathbb{Z}^n$. □

If a lattice can be obtained from another by rotation, reflection and uniform change of scale, we say they are *equivalent*, written $\cong$ [9]. Any n-dimensional lattice $\mathcal{L}_n$ has a *dual* lattice given by

$$\mathcal{L}_n^* := \{\boldsymbol{x} \in \mathbb{R}^m : \boldsymbol{x} \cdot \boldsymbol{u} \in \mathbb{Z}, \forall \boldsymbol{u} \in \mathcal{L}_n\}. \tag{1}$$

If $\mathbf{G}$ is a square generator matrix of $\mathcal{L}_n$, then $\mathbf{G}^{-t}$ is a square generator matrix of $\mathcal{L}_n^*$ [9]. If $\mathbf{G}$ is the generator matrix of $\mathcal{L}_n$, an orthogonal matrix $\mathbf{B}$ is in the *symmetry group* (or *automorphism group*) $\mathrm{Aut}(\mathcal{L}_n)$, i.e. the set of *isometries* with one invariant lattice point that transform $\mathcal{L}_n$ to itself, if and only if there is a unimodular matrix $\mathbf{U} \in \mathbb{Z}^{n\times n}$ such that [9] $\mathbf{GU} = \mathbf{BG}$. Therefore, the order of $\mathrm{Aut}(\mathcal{L}_n)$ tells how symmetric a lattice is; $\mathcal{L}_n$ and $\mathcal{L}_n^*$ have the same symmetry group.

In many geometric problems related to lattices, *root lattices* defined via *root systems* [9] provide good solutions due to their inherent symmetry. Symmetry also makes them good sampling lattices for the signals with isotropic frequencies. In this paper we focus on the root lattices $\mathcal{A}_n$ and $\mathcal{A}_n^*$.

Let $\text{Ш}_{\mathbf{G}}(\boldsymbol{x}) := \sum_{\boldsymbol{k}\in\mathbb{Z}^n} \delta(\boldsymbol{x} - \mathbf{G}\boldsymbol{k})$ be the Dirac comb function that samples a function f on the lattice $\mathbf{G}\mathbb{Z}^n$, $\mathbf{G} \in \mathbb{R}^{n\times n}$, and denote by $\widehat{f}(\boldsymbol{\omega}) = \mathcal{F}\{f\}(\boldsymbol{\omega})$ the Fourier transform of f. Since [14]

$$\mathcal{F}\{f\text{Ш}_{\mathbf{G}}\}(\boldsymbol{\omega}) = \frac{1}{|\det \mathbf{G}|} \sum_{\boldsymbol{k}\in\mathbb{Z}^n} \widehat{f}(\boldsymbol{\omega} - \mathbf{G}^{-t}\boldsymbol{k}), \tag{2}$$

the Fourier transform of the sampling $f\text{Ш}_{\mathbf{G}}$ replicates $\widehat{f}(\boldsymbol{\omega})$ on $\mathbf{G}^{-t}\mathbb{Z}^n$, the (scaled) dual lattice of $\mathbf{G}\mathbb{Z}^n$. The choice of $\mathbf{G}$ determines the 'packing density' as explained next.

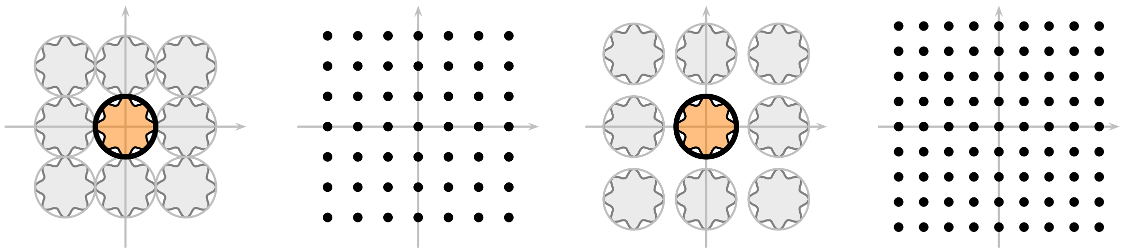

(a) $\mathcal{F}\left\{f\text{Ш}_{\mathbf{G}_1}\right\}(\boldsymbol{\omega})$ (b) $f\text{Ш}_{\mathbf{G}_1}(\boldsymbol{x})$ (c) $\mathcal{F}\left\{f\text{Ш}_{\mathbf{G}_2}\right\}(\boldsymbol{\omega})$ (d) $f\text{Ш}_{\mathbf{G}_2}(\boldsymbol{x})$

Figure 2: Lattice packing (frequency domain) and efficient sampling (primal domain). The *maroon, bold* star shapes in (a) and (c) represent the band-limited Fourier transform $\mathcal{F}\{f\}$ of a given function f; the *gray* replicas are the transforms $\mathcal{F}\left\{f\text{Ш}_{\mathbf{G}_1}\right\}$ and $\mathcal{F}\left\{f\text{Ш}_{\mathbf{G}_2}\right\}$ of samples $f\text{Ш}_{\mathbf{G}_1}$ and $f\text{Ш}_{\mathbf{G}_2}$ on lattices with generator matrices, $\mathbf{G}_1$ and $\mathbf{G}_2$ respectively. From both transforms, the original signal can be reconstructed by removing the replicas with a low-pass filter (thick circle) and applying the inverse Fourier transform. But the denser packing of replicas in Figure (a) is more efficient since it corresponds to a sparser sampling lattice in the primal space, Figure (b).

$\mathbb{Z}^n$	$\mathcal{A}_n$	$\mathcal{A}_n^*$	$\mathcal{D}_n$ $(n \geq 3)$	$\mathcal{D}_n^*$ $(n \geq 3)$
2^{-n}	$2^{-n/2}(n+1)^{-1/2}$	$\dfrac{n^{n/2}}{2^n(n+1)^{(n-1)/2}}$	$2^{-(n+2)/2}$	$\begin{cases} 3^{1.5}2^{-5} & (n=3) \\ 2^{-(n-1)} & (n>3) \end{cases}$

Table 1: Center density of several root lattices. $\mathcal{D}_n := \{(i_1, \ldots, i_n) : \sum i_k \text{ is even}\}$ [9]. See Section 3.2 for the definition of $\mathcal{A}_n$ and $\mathcal{A}_n^*$.

The *sphere packing problem*, "how densely can we pack identical spheres in $\mathbb{R}^n$?", is one of the oldest problems in geometry [9]. The *lattice packing* problem is to find the lattice that induces the densest sphere packing when the spheres are located at the lattice points. The lattice packing problem is closely related to the *optimal sampling lattice* for multi-dimensional signal processing. Assuming the frequency of the input signal is isotropic and band-limited, we can reconstruct the original signal using a sphere-shaped filter in the frequency domain (Figure 2(a) and 2(c)). Since the lattice in the frequency domain is the dual of the sampling lattice, the more densely we can pack the spheres (reconstruction filters) in the frequency domain, the sparser a sampling lattice we can choose in the space domain to reconstruct the original signal (Figure 2). Therefore, for input signals with isotropic band-limited frequencies, the n-dimensional optimal sampling lattice is the *dual of the n-dimensional optimal sphere packing lattice* [17, 25, 15].

The *density* of a lattice packing is the proportion of the space occupied by the spheres when packed. The *center density* of a lattice is the number of the lattice points per unit volume, which can be obtained by dividing its density by the volume of the unit sphere [9]. Therefore, larger (center) density implies that *its dual is a more efficient sampling lattice.* Table 1 and Figure 3 respectively show the center density and the density of several important root lattices. Both imply poorer sampling efficiency of the Cartesian lattice $\mathbb{Z}^n$ compared to other root lattices.

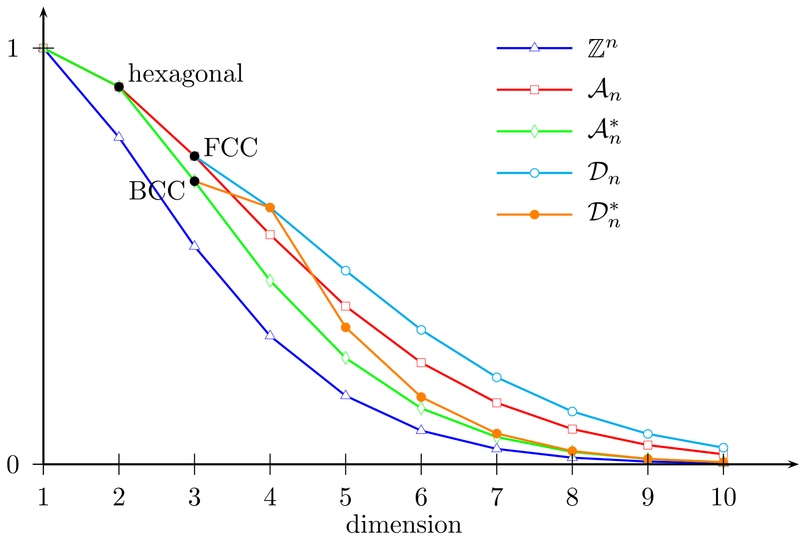

Figure 3: Density of several root lattices up to dimension 10.

3.2. The root lattices $\mathcal{A}_n$ and $\mathcal{A}_n^*$ as subsets of $\mathbb{R}^{n+1}$

The (n-dimensional) lattice $\mathcal{A}_n$ embedded in $\mathbb{R}^{n+1}$ has points $\{\boldsymbol{x} \in \mathbb{Z}^{n+1} : \mathbf{j} \cdot \boldsymbol{x} = \mathbf{0}\} = \mathbb{Z}^{n+1} \cap H_{\mathbf{j}}^n$ [28] and can be generated by the $(n+1) \times n$ matrix [9, page 109]

$$\mathbf{A}_{\mathrm{C}} := \begin{bmatrix} -1 & & & & & \\ 1 & -1 & & & & \\ & 1 & \ddots & & & \\ & & \ddots & -1 & & \\ & & & 1 & -1 \\ & & & & 1 \end{bmatrix} \in \mathbb{Z}^{(n+1)\times n}. \tag{3}$$

We can easily check (see also [9, page 115]) that its dual $\mathcal{A}_n^*$ can be generated by the $(n+1) \times n$ matrix

$$\mathbf{A}_{\mathrm{C}}^* := \begin{bmatrix} 1 & \cdots & 1 & -n/(n+1) \\ -1 & & & 1/(n+1) \\ & \ddots & & \vdots \\ & & -1 & 1/(n+1) \\ & & & 1/(n+1) \end{bmatrix} = \begin{bmatrix} \mathbf{j}^t & -n/(n+1) \\ -\mathbf{I}_{n-1} & \mathbf{j}/(n+1) \\ \mathbf{0}^t & 1/(n+1) \end{bmatrix} \in \mathbb{R}^{(n+1)\times n}.$$

Some examples of $\mathcal{A}_n$ and $\mathcal{A}_n^*$ are:

- $\mathcal{A}_2$ and $\mathcal{A}_2^*$ are equivalent to the hexagonal lattice.
- $\mathcal{A}_3 \cong \mathcal{D}_3$ is equivalent to the FCC (Face-Centered Cubic) lattice.
- $\mathcal{A}_3^* \cong \mathcal{D}_3^*$ is equivalent to the BCC (Body-Centered Cubic) lattice.

$\mathcal{A}_n^*$ is the optimal sampling lattice in 2- and in 3-dimensions [30, 32, 17, 16, 25, 18, 29, 15]. In dimensions higher than 3, Figure 3 shows that $\mathcal{A}_n$ packs spheres better than the Cartesian lattice, making $\mathcal{A}_n^*$ a better sampling lattice than $\mathbb{Z}^n$.

The basis of $\mathcal{A}_n$ can be taken from an n-dimensional equilateral simplex.

Lemma 2 (Classic geometric construction of $\mathcal{A}_n$ and $\mathcal{A}_n^*$ in $\mathbb{R}^{n+1}$)**.**

(i) Let σ_n be an equilateral *n-dimensional simplex one of whose vertices is located at the origin. Then the n edges of σ_n emanating from the origin form a basis of a lattice equivalent to $\mathcal{A}_n$.*

(ii) $\mathcal{A}_n^*$ can be generated by the non-invertible elementary matrix

$$\mathbf{P}_{n+1} := \mathbf{I}_{n+1} - \frac{1}{n+1}\mathbf{J}_{n+1} \in \mathbb{R}^{(n+1)\times(n+1)}, \tag{4}$$

the orthogonal projection of the $(n+1)$-dimensional Cartesian lattice $\mathbb{Z}^{n+1}$ along the diagonal direction $\mathbf{j}$.

Proof. (i) Let

$$\mathbf{U} := \begin{bmatrix} 1 & & & \\ 1 & 1 & & \\ \vdots & \vdots & \ddots & \\ 1 & 1 & \cdots & 1 \end{bmatrix} \in \mathbb{Z}^{n\times n}, \quad \text{hence} \quad \mathbf{U}^{-1} = \begin{bmatrix} 1 & & & & \\ -1 & 1 & & & \\ & -1 & \ddots & & \\ & & \ddots & 1 & \\ & & & -1 & 1 \end{bmatrix}.$$

By Lemma 1,

$$\mathbf{A}_{\mathrm{C}}\mathbf{U} = \begin{bmatrix} -\mathbf{I}_n \\ \mathbf{j}^t \end{bmatrix} \in \mathbb{Z}^{(n+1)\times n}, \tag{5}$$

also generates $\mathcal{A}_n$. Since

$$\begin{cases} \|\boldsymbol{v}\|_2 = \sqrt{2} & \forall \boldsymbol{v} \in \mathbf{A}_{\mathrm{C}}\mathbf{U} \\ \|\boldsymbol{v}_j - \boldsymbol{v}_k\|_2 = \sqrt{2} & \forall \boldsymbol{v}_j, \boldsymbol{v}_k \in \mathbf{A}_{\mathrm{C}}\mathbf{U}, \boldsymbol{v}_j \neq \boldsymbol{v}_k, \end{cases}$$

the simplex $\operatorname{conv}(\{\mathbf{0}\} \cup \bigcup_{\boldsymbol{v}\in\mathbf{A}_{\mathrm{C}}\mathbf{U}}\{\boldsymbol{v}\})$ is equilateral hence equivalent to any σ_n.

(ii) For

$$\mathbf{U} := \begin{bmatrix} \mathbf{0} & -\mathbf{I}_{n-1} \\ -1 & -\mathbf{j}^t \end{bmatrix} \in \mathbb{Z}^{n\times n} \quad \text{hence} \quad \mathbf{U}^{-1} = \begin{bmatrix} \mathbf{j}^t & -1 \\ -\mathbf{I}_{n-1} & \mathbf{0} \end{bmatrix},$$

we verify that

$$\mathbf{A}_{\mathrm{P}}^* := \mathbf{A}_{\mathrm{C}}^*\mathbf{U} = \frac{1}{n+1}\begin{bmatrix} (n+1)\mathbf{I}_n - \mathbf{J}_n \\ -\mathbf{j}^t \end{bmatrix} \in \mathbb{R}^{(n+1)\times n}, \tag{6}$$

where $\mathbf{A}_{\mathrm{P}}^*$ is the matrix of the first n columns of $\mathbf{P}_{n+1}$. The last column of $\mathbf{P}_{n+1}$ is an integer linear combination of the first n columns, $\mathbf{A}_{\mathrm{P}}^*$. By Lemma 1, the claim follows.

□

3.3. The box-splines M_r

We briefly review the later-referenced facts about box-splines following de Boor *et al.* [13] and introduce the box-splines M_r.

A box-spline $M_{\boldsymbol{\Xi}}$ is defined by its *matrix (multi-set) of directions* $\boldsymbol{\Xi}$. Unless mentioned specifically, we assume that $\boldsymbol{\Xi} \in \mathbb{Z}^{n\times m}$ $(m \geq n)$ and $\operatorname{ran}\boldsymbol{\Xi} = \mathbb{R}^n$. Geometrically, the value at $x \in \operatorname{ran}\boldsymbol{\Xi}$ of the box-spline $M_{\boldsymbol{\Xi}}$ is defined as the (normalized) shadow density of the $(m-n)$-dimensional volume of the intersection between the preimage of $\boldsymbol{x}$ and the m-dimensional half-open unit cube $\square := [0..1)^m$: [13, (I.3)] (see e.g., Figure 1)

$$M_{\boldsymbol{\Xi}}(\boldsymbol{x}) := \mathrm{vol}_{m-n}\left(\boldsymbol{\Xi}^{-1}\{\boldsymbol{x}\} \cap \square\right)/|\det \boldsymbol{\Xi}| \tag{7}$$

where $\boldsymbol{\Xi}$ is viewed as a linear transformation $\boldsymbol{\Xi} : \mathbb{R}^m \to \mathbb{R}^n$ and the preimage of $\boldsymbol{x}$ is defined as [13, (I.7)]

$$\boldsymbol{\Xi}^{-1}\{\boldsymbol{x}\} = \boldsymbol{\Xi}^t \left(\boldsymbol{\Xi}\boldsymbol{\Xi}^t\right)^{-1}\{\boldsymbol{x}\} + \ker \boldsymbol{\Xi}. \tag{8}$$

Let $\mathbb{H}(\boldsymbol{\Xi})$ be the collection of all the hyperplanes spanned by the columns of $\boldsymbol{\Xi}$. We call the shifts of all the hyperplanes in $\mathbb{H}(\boldsymbol{\Xi})$ **knot planes**: [13, page 16]

$$\Gamma(\boldsymbol{\Xi}) := \bigcup_{H \in \mathbb{H}(\boldsymbol{\Xi})} H + \mathbb{Z}^n. \tag{9}$$

The box-spline $M_{\boldsymbol{\Xi}}$ with $\boldsymbol{\Xi} \in \mathbb{Z}^{n\times m}$ is a **piecewise polynomial** function on $\mathrm{ran}\boldsymbol{\Xi}$. It is delineated by the knot planes and is of degree less than or equal to [13, page 9]

$$k(\boldsymbol{\Xi}) := m - \dim \mathrm{ran}\boldsymbol{\Xi}. \tag{10}$$

Specifically, $k(\boldsymbol{\Xi}) = m - n$ if $\mathrm{ran}\boldsymbol{\Xi} = \mathbb{R}^n$.

The **centered box-spline** $M^{c}_{\boldsymbol{\Xi}}$ of $M_{\boldsymbol{\Xi}}$ is [13, (I.21)]

$$M^{c}_{\boldsymbol{\Xi}} := M_{\boldsymbol{\Xi}}(\cdot + \sum_{\boldsymbol{\xi}\in\boldsymbol{\Xi}} \boldsymbol{\xi}/2). \tag{11}$$

Given an invertible **linear map** $\mathbf{L}$ on $\mathbb{R}^n$, [13, (I.23)]

$$M_{\boldsymbol{\Xi}} = |\det \mathbf{L}| M_{\mathbf{L}\boldsymbol{\Xi}} \circ \mathbf{L}. \tag{12}$$

The **Fourier transform** of $M_{\boldsymbol{\Xi}}$ is [13, (I.17)]

$$\widehat{M_{\boldsymbol{\Xi}}}(\boldsymbol{\omega}) := \mathcal{F}\{M_{\boldsymbol{\Xi}}\}(\boldsymbol{\omega}) = \prod_{\boldsymbol{\xi}\in\boldsymbol{\Xi}} \frac{1-\exp(-i\boldsymbol{\xi}\cdot\boldsymbol{\omega})}{i\boldsymbol{\xi}\cdot\boldsymbol{\omega}}, \qquad i := \sqrt{-1}. \tag{13}$$

If $M_{\boldsymbol{\Xi}}$ is *centered*, i.e. if $M_{\boldsymbol{\Xi}} = M^{c}_{\boldsymbol{\Xi}}$, then [13, page 11]

$$\widehat{M_{\boldsymbol{\Xi}}}(\boldsymbol{\omega}) = \prod_{\boldsymbol{\xi}\in\boldsymbol{\Xi}} \mathrm{sinc}(\boldsymbol{\xi}\cdot\boldsymbol{\omega}). \tag{14}$$

By [13, page 9], the (closed) **support** of $M_{\boldsymbol{\Xi}}$ consists of the set

$$\overline{\mathrm{supp} M_{\boldsymbol{\Xi}}} = \boldsymbol{\Xi}\,\blacksquare = \{\sum_{\boldsymbol{\xi}\in\boldsymbol{\Xi}} \boldsymbol{\xi} \boldsymbol{t}_{\boldsymbol{\xi}} : 0 \le \boldsymbol{t}_{\boldsymbol{\xi}} \le 1\} \tag{15}$$

where $\blacksquare := [0..1]^m$ is the closed unit cube and $\boldsymbol{t}_{\boldsymbol{\xi}}$ is the element of $\boldsymbol{t}$ associated with $\boldsymbol{\xi}$ by $\boldsymbol{\Xi}\boldsymbol{t}$. Assuming $\mathrm{ran}\boldsymbol{\Xi} = \mathbb{R}^n$, the set of all *bases* of $\boldsymbol{\Xi}$ is denoted [13, page 8]

$$\mathcal{B}(\boldsymbol{\Xi}) := \{\mathbf{Z} \subseteq \boldsymbol{\Xi} : \#\mathbf{Z} = \mathrm{rank}\mathbf{Z} = n\}. \tag{16}$$

The support of $M_{\boldsymbol{\Xi}}$ is composed of the parallelepipeds spanned by $\mathbf{Z} \in \mathcal{B}(\boldsymbol{\Xi})$: For $\mathrm{ran}\boldsymbol{\Xi} = \mathbb{R}^n$ there exists points $\boldsymbol{\alpha}_{\mathbf{Z}} \in \boldsymbol{\Xi}\{0,1\}^m$, $\mathbf{Z} \in \mathcal{B}(\boldsymbol{\Xi})$, so that $\boldsymbol{\Xi}\,\blacksquare$ is the essentially disjoint union of the sets [13, I.53]

$$\mathbf{Z}\,\blacksquare + \boldsymbol{\alpha}_{\mathbf{Z}}, \quad \mathbf{Z} \in \mathcal{B}(\boldsymbol{\Xi}). \tag{17}$$

The **cardinal spline space** [13, (II.1)]

$$S_{\boldsymbol{\Xi}} := \operatorname{span}\left(M_{\boldsymbol{\Xi}}(\cdot - \boldsymbol{j})\right)_{\boldsymbol{j}\in\mathbb{Z}^n} \tag{18}$$

is the spline space spanned by the shifts of $M_{\boldsymbol{\Xi}}$ on $\mathbb{Z}^n$. The sequence $\left(M_{\boldsymbol{\Xi}}(\cdot - \boldsymbol{j})\right)_{\boldsymbol{j}\in\mathbb{Z}^n}$ is **linearly independent** if and only if $\boldsymbol{\Xi}$ is *unimodular* [13, page 41].

The map

$$M_{\boldsymbol{\Xi}}*' : f \mapsto \sum_{\boldsymbol{j}\in\mathbb{Z}^n} M_{\boldsymbol{\Xi}}(\cdot - \boldsymbol{j}) f(\boldsymbol{j}) \tag{19}$$

reproduces the polynomials in $\Pi_{M_{\boldsymbol{\Xi}}} := \Pi \cap S_{\boldsymbol{\Xi}}$ where Π is the set of all the polynomials on $\mathbb{R}^n$ [13, page 52]. Specifically, $\Pi_{m(\boldsymbol{\Xi})} \subseteq \Pi_{M_{\boldsymbol{\Xi}}}$ where

- Π_α is the set of polynomials of (total) degree up to α,
- $m(\boldsymbol{\Xi}) := \min\{\#\mathbf{Z} : \mathbf{Z} \in \mathcal{A}(\boldsymbol{\Xi})\} - 1$ and
- $\mathcal{A}(\boldsymbol{\Xi}) := \{\mathbf{Z} \subseteq \boldsymbol{\Xi} : \boldsymbol{\Xi}\backslash\mathbf{Z} \text{ does not span}\}$.

In other words, $M_{\boldsymbol{\Xi}}*'$ can reproduce all the polynomials up to (total) degree $m(\boldsymbol{\Xi})$. The following **quasi-interpolant** $Q_{\boldsymbol{\Xi}}$ for a box-spline $M_{\boldsymbol{\Xi}}$ provides a fast way of approximating a function f with a spline $Q_{\boldsymbol{\Xi}} f \in S_{\boldsymbol{\Xi}}$ [13]. Here we focus on the quasi-interpolant that provides the maximal **approximation order** $m(\boldsymbol{\Xi}) + 1$: [13, page 72]

$$(Q_{\boldsymbol{\Xi}} f)(\boldsymbol{x}) := \sum_{\boldsymbol{j}\in\mathbb{Z}^n} M_{\boldsymbol{\Xi}}(\boldsymbol{x} - \boldsymbol{j}) \lambda_{\boldsymbol{\Xi}}\left(f(\cdot + \boldsymbol{j})\right) \tag{20}$$

where $\lambda_{\boldsymbol{\Xi}}$ is the linear functional [13, (III.22)]

$$\lambda_{\boldsymbol{\Xi}} f := \sum_{|\boldsymbol{\alpha}|\le m(\boldsymbol{\Xi})} g_{\boldsymbol{\alpha}}(\mathbf{0}) \left(D^{\boldsymbol{\alpha}} f\right)(\mathbf{0}) \tag{21}$$

and $\boldsymbol{\alpha} \in \mathbb{Z}_+^n$ is a *multi-index* with $|\boldsymbol{\alpha}| := \sum_{\nu=1}^n \boldsymbol{\alpha}(\nu)$. The **Appell sequence** $\{g_{\boldsymbol{\alpha}}\}$ in (21) can be computed either recursively as

$$\begin{cases} g_{\mathbf{0}} := [\![]\!]^{\mathbf{0}} \\ g_{\boldsymbol{\alpha}} := [\![]\!]^{\boldsymbol{\alpha}} - \sum_{\boldsymbol{\beta}\ne\boldsymbol{\alpha}} (\mu_{\boldsymbol{\Xi}} [\![]\!]^{\boldsymbol{\alpha}-\boldsymbol{\beta}}) g_{\boldsymbol{\beta}} \end{cases} \qquad ([13, (III.19)])$$

where

$$\mu_{\boldsymbol{\Xi}}(f) := \sum_{\boldsymbol{j}} M_{\boldsymbol{\Xi}}(\boldsymbol{j}) f(-\boldsymbol{j}), \tag{22}$$

or from the Fourier transform $\widehat{M_{\boldsymbol{\Xi}}}$: [13, (III.34)]

$$g_{\boldsymbol{\alpha}}(\mathbf{0}) = \left([\![-iD]\!]^{\boldsymbol{\alpha}} \left(1/\widehat{M_{\boldsymbol{\Xi}}}\right)\right)(\mathbf{0}). \tag{23}$$

Note that $[\![]\!]^{\boldsymbol{\alpha}}$ is the *normalized $\boldsymbol{\alpha}$-power function*

$$[\![x]\!]^{\boldsymbol{\alpha}} := \boldsymbol{x}^{\boldsymbol{\alpha}}/\boldsymbol{\alpha}! := \prod_{\nu=1}^n \frac{\boldsymbol{x}(\nu)^{\boldsymbol{\alpha}(\nu)}}{\boldsymbol{\alpha}(\nu)!}.$$

The Box-Spline M_r. Box-splines defined by possibly repeated $(n+1)$ distinct convolution directions are also called *box-splines on the $(n+1)$-directional mesh* [1]. Given the $n \times (n+1)$ matrix of directions

$$\mathbf{T}_1 := \begin{bmatrix} \mathbf{I}_n & -\mathbf{j} \end{bmatrix} = \begin{bmatrix} \mathbf{i}_1 & \cdots & \mathbf{i}_n & -\mathbf{j} \end{bmatrix} \in \mathbb{Z}^{n\times(n+1)}, \tag{24}$$

the box-spline *with multiplicity* r in each direction is defined by the $n \times r(n+1)$ matrix of directions $\mathbf{T}_r$ [13, page 80] with the multi-set

$$\mathbf{T}_r := \bigcup_{j=1}^{r} \mathbf{T}_1 \quad \text{and we abbreviate} \quad M_r := M_{\mathbf{T}_r}. \tag{25}$$

As pointed out in Section 2, this family of box-splines has been widely used. Since $\mathbf{T}_1 = \begin{bmatrix} 1 & -1 \end{bmatrix}$ in the univariate case, M_r can be viewed as a generalization of the uniform B-splines of odd degree to arbitrary dimensions.

4. Box-splines on Non-Cartesian Lattices

By (12), given a square generator matrix $\mathbf{G}$, any weighted sum of the shifts of the (scaled) box-spline

$$\widetilde{M}_{\boldsymbol{\Xi}} := |\det \mathbf{G}| M_{\mathbf{G}\boldsymbol{\Xi}} \tag{26}$$

on the (possibly non-Cartesian) lattice $\mathbf{G}\mathbb{Z}^n$ can be expressed as a weighted sum of the shifts of $M_{\boldsymbol{\Xi}}$ on the Cartesian lattice $\mathbb{Z}^n$ by *change of variables*:

$$\sum_{\boldsymbol{j} \in \mathbf{G}\mathbb{Z}^n} \widetilde{M}_{\boldsymbol{\Xi}}(\cdot - \boldsymbol{j}) a(\boldsymbol{j}) = \sum_{\boldsymbol{k} \in \mathbb{Z}^n} M_{\boldsymbol{\Xi}}(\mathbf{G}^{-1} \cdot - \boldsymbol{k}) a(\mathbf{G}\boldsymbol{k}) \tag{27}$$

where $a : \mathbf{G}\mathbb{Z}^n \to \mathbb{R}$ is the mesh function (spline coefficients) on $\mathbf{G}\mathbb{Z}^n$. In the bivariate setting, de Boor and Höllig [10, page 650] already pointed to this relationship.

We denote the spline space spanned by the shifts of $\widetilde{M}_{\boldsymbol{\Xi}}$ on $\mathbf{G}\mathbb{Z}^n$ by

$$S_{\boldsymbol{\Xi}}^{\mathbf{G}} := \operatorname{span}\left(\widetilde{M}_{\boldsymbol{\Xi}}(\cdot - \boldsymbol{j})\right)_{\boldsymbol{j} \in \mathbf{G}\mathbb{Z}^n}.$$

This notation becomes consistent with (18) by omitting $\mathbf{G} = \mathbf{I}_n$ and defining

$$S_{\boldsymbol{\Xi}} := S_{\boldsymbol{\Xi}}^{\mathbf{I}_n}.$$

Lemma 3 (Quasi-interpolant). *Let $D_{\mathbf{G}}^{\boldsymbol{\alpha}} := \prod_{\boldsymbol{v} \in \mathbf{G}} D_{\boldsymbol{v}}^{\boldsymbol{\alpha}_{\boldsymbol{v}}}$ be the composition of directional derivatives $D_{\boldsymbol{v}} := \sum_{j=1}^{n} \boldsymbol{v}(j) D_j$ along the columns of $\mathbf{G}$ and $\{g_{\boldsymbol{\alpha}}\}$ the Appell sequence of $\lambda_{\boldsymbol{\Xi}}$ (21). The quasi-interpolant $Q_{\boldsymbol{\Xi}}^{\mathbf{G}}$ for $S_{\boldsymbol{\Xi}}^{\mathbf{G}}$ defined by the functional*

$$\lambda_{\boldsymbol{\Xi}}^{\mathbf{G}}\left(f\left(\cdot + \boldsymbol{j}\right)\right) := \lambda_{\boldsymbol{\Xi}}\left(\left(f \circ \mathbf{G}\right)\left(\cdot + \mathbf{G}^{-1} j\right)\right) \tag{28}$$

$$= \sum_{|\boldsymbol{\alpha}| \leq m(\boldsymbol{\Xi})} g_{\boldsymbol{\alpha}}(\mathbf{0}) \left(D_{\mathbf{G}}^{\boldsymbol{\alpha}} f\right)(\boldsymbol{j}), \quad \boldsymbol{j} \in \mathbf{G}\mathbb{Z}^n \tag{29}$$

provides the same maximal approximation power as does $Q_{\boldsymbol{\Xi}}$ defined by $\lambda_{\boldsymbol{\Xi}}$ for $S_{\boldsymbol{\Xi}}$.

Proof. If we define

$$\left(Q_{\boldsymbol{\Xi}}^{\mathbf{G}} f\right)(x) := \left(Q_{\boldsymbol{\Xi}}\left(f \circ \mathbf{G}\right)\right)\left(\mathbf{G}^{-1} \boldsymbol{x}\right)$$

then, since $f = f \circ \mathbf{G} \circ \mathbf{G}^{-1}$,

$$\left(f - Q_{\boldsymbol{\Xi}}^{\mathbf{G}} f\right)(\boldsymbol{x}) = \left(\left(f \circ \mathbf{G}\right) - Q_{\boldsymbol{\Xi}}\left(f \circ \mathbf{G}\right)\right)\left(\mathbf{G}^{-1} \boldsymbol{x}\right) = \left(\widetilde{f} - Q_{\boldsymbol{\Xi}} \widetilde{f}\right)(\widetilde{\boldsymbol{x}}),$$

for $\widetilde{f} := f \circ \mathbf{G}$ and $\widetilde{\boldsymbol{x}} := \mathbf{G}^{-1}\boldsymbol{x}$, i.e., $Q_{\boldsymbol{\Xi}}^{\mathbf{G}}$ has the same approximation power as $Q_{\boldsymbol{\Xi}}$. Since

$$\begin{aligned}
\left(Q_{\boldsymbol{\Xi}}\left(f \circ \mathbf{G}\right)\right)\left(\mathbf{G}^{-1}\boldsymbol{x}\right) &= \sum_{\boldsymbol{k}\in\mathbb{Z}^n} M_{\boldsymbol{\Xi}}(\mathbf{G}^{-1}\boldsymbol{x}-\boldsymbol{k})\lambda_{\boldsymbol{\Xi}}\left(\left(f\circ\mathbf{G}\right)\left(\cdot+\boldsymbol{k}\right)\right) \\
&= \sum_{\boldsymbol{j}\in\mathbf{G}\mathbb{Z}^n} |\det\mathbf{G}| M_{\mathbf{G}\boldsymbol{\Xi}}(\boldsymbol{x}-\boldsymbol{j})\lambda_{\boldsymbol{\Xi}}\left(\left(f\circ\mathbf{G}\right)\left(\cdot+\mathbf{G}^{-1}\boldsymbol{j}\right)\right),
\end{aligned}$$

and

$$D_{\boldsymbol{k}}\left(f\circ\mathbf{G}\right) = \lim_{h\to 0}\frac{f\left(\mathbf{G}\cdot+h\mathbf{G}\mathbf{i}_{\boldsymbol{k}}\right)-f\left(\mathbf{G}\cdot\right)}{h} = \left(D_{\mathbf{G}\mathbf{i}_{\boldsymbol{k}}}f\right)\circ\mathbf{G},$$

the corresponding functional $\lambda_{\boldsymbol{\Xi}}^{\mathbf{G}}$ is for $\boldsymbol{j}\in\mathbf{G}\mathbb{Z}^n$

$$\begin{aligned}
\lambda_{\boldsymbol{\Xi}}^{\mathbf{G}}\left(f\left(\cdot+\boldsymbol{j}\right)\right) &= \lambda_{\boldsymbol{\Xi}}\left(\left(f\circ\mathbf{G}\right)\left(\cdot+\mathbf{G}^{-1}\boldsymbol{j}\right)\right) \\
&= \sum_{|\boldsymbol{\alpha}|\le m(\boldsymbol{\Xi})} g_{\boldsymbol{\alpha}}(\mathbf{0})\left(D^{\boldsymbol{\alpha}}\left(f\circ\mathbf{G}\right)\right)\left(\mathbf{G}^{-1}\boldsymbol{j}\right) && \text{(by (21))} \\
&= \sum_{|\boldsymbol{\alpha}|\le m(\boldsymbol{\Xi})} g_{\boldsymbol{\alpha}}(\mathbf{0})\left(D_{\mathbf{G}}^{\boldsymbol{\alpha}}f\right)(\boldsymbol{j}).
\end{aligned}$$

□

5. The Representation $\mathbf{A}^*\mathbb{Z}^n$ of $\mathcal{A}_n^*$

Next, in Section 5.1, we show the need for a non-standard representation of the efficient reconstruction lattice $\mathcal{A}_n^*$. This representation, $\mathbf{A}^*\mathbb{Z}^n$, is introduced in Section 5.2 and Section 5.3 defines the family of box-splines $M_r^* := M_r \circ \mathbf{A}^{*-1}$ on $\mathcal{A}_n^*$.

5.1. Bias of box-splines M_1

The box-spline family M_r and the $\mathcal{A}_n^*$ lattice have a close relationship that becomes apparent when we compare the spline spaces

$$S_{\mathbf{P}_{n+1}}^{\mathbf{A}_{\mathrm{P}}^*} := \operatorname{span}(M_1^+(\cdot-\boldsymbol{j}))_{\boldsymbol{j}\in\mathbf{A}_{\mathrm{P}}^*\mathbb{Z}^n} \quad \text{and} \quad S_{\mathbf{T}_1} := \operatorname{span}(M_1(\cdot-\boldsymbol{j}))_{\boldsymbol{j}\in\mathbb{Z}^n}$$

where $M_1^+ := |\det\mathbf{A}_{\mathrm{P}}^*| M_{\mathbf{P}_{n+1}}$ and $\mathbf{A}_{\mathrm{P}}^*$ was defined in (6). Since

$$\mathbf{A}_{\mathrm{P}}^{*\,t}\mathbf{A}_{\mathrm{P}}^* = \mathbf{I}_n - \mathbf{J}_n/(n+1) = \mathbf{I}_n - \mathbf{j}\mathbf{j}^t/(n+1) \tag{30}$$

and by Sylvester's determinant theorem,

$$\det(\mathbf{I}_n - \mathbf{j}\mathbf{j}^t/(n+1)) = \det(\mathbf{I}_1 - n/(n+1)) = \frac{1}{n+1}, \tag{31}$$

$|\det\mathbf{A}_{\mathrm{P}}^*| := \sqrt{\det\left(\mathbf{A}_{\mathrm{P}}^{*\,t}\mathbf{A}_{\mathrm{P}}^*\right)} = 1/\sqrt{n+1}$. Since $\mathbf{P}_{n+1} = \mathbf{I}_{n+1} - \mathbf{J}_{n+1}/(n+1) = \mathbf{A}_{\mathrm{P}}^*\mathbf{T}_1$, the two spaces are related by

$$\sum_{\boldsymbol{j}\in\mathbf{A}_{\mathrm{P}}^*\mathbb{Z}^n} M_1^+(\cdot-\boldsymbol{j})a(\boldsymbol{j}) = \sum_{\boldsymbol{k}\in\mathbb{Z}^n} M_1(\mathbf{A}_{\mathrm{P}}^{*\,-1}\cdot-\boldsymbol{k})a(\mathbf{A}_{\mathrm{P}}^*\boldsymbol{k})$$

where $\mathbf{A}_{\mathrm{P}}^{*\,-1}$ is defined in the manner of (8). The equation is similar to (27) but $\mathbf{A}_{\mathrm{P}}^*$ is not a square matrix! The spline space $S_{\mathbf{T}_1}$, though widely used, corresponds to the Cartesian domain lattice that has poorer sampling efficiency compared to other root lattices, as pointed out in Section 3.1. Moreover, while M_1^+

spline space	$S_{\mathbf{T}_1}$ M_1 on $\mathbb{Z}^n$	$S_{\mathbf{P}_{n+1}}^{\mathbf{A}_{\mathrm{P}}^*}$ M_1^+ on $\mathbf{A}_{\mathrm{P}}^*\mathbb{Z}^n$	$S_{\mathbf{T}_1^*}^{\mathbf{A}^*}$ M_1^* on $\mathbf{A}^*\mathbb{Z}^n$
symmetric box-spline		✓	✓
domain lattice is $\mathcal{A}_n^*$		✓	✓
domain is $\mathbb{R}^n$	✓		✓

Table 2: Box-spline spaces related by change of variables.

is symmetric, as shown below, M_1 is not (Figure 4), since, according to (30), $\mathbf{A}_{\mathrm{P}}^*$ is not an orthonormal transformation:

$$\mathbf{A}_{\mathrm{P}}^{*\,t}\mathbf{A}_{\mathrm{P}}^* = \mathbf{I}_n - \frac{1}{n+1}\mathbf{J}_n \neq \mathbf{I}_n. \tag{32}$$

Therefore M_1 is a biased reconstruction filter.

By contrast, the domain lattice of the box-spline M_1^+ is the efficient sampling lattice $\mathcal{A}_n^*$ and M_1^+ is symmetric since the directions, i.e. the columns of $\mathbf{P}_{n+1}$, are

- isometric: they have the same lengths and
- isotropic: the inner product (hence the angle) between any two directions is the same.

The support of M_1^+ inherits the symmetry of $\mathcal{A}_n^*$ (or $\mathcal{A}_n$) since the directions in $\mathbf{P}_{n+1}$ are taken from the (non-parallel) directions from the origin to the nearest lattice points (of which there are $2(n+1)$, the *kissing number* of $\mathcal{A}_n^*$ [9]).

The shifts of M_1^+ are the box-splines obtained by projecting a slab as shown in Figure 1. The lattice $\mathcal{A}_n^*$ on the hyperplane $H_{\mathbf{j}}^n \subsetneq \mathbb{R}^{n+1}$ partitions the slab. The next lemma shows that this partition can serve as an alternate preimage of (the shifts of) $\overline{\mathrm{supp} M_1}$, besides the box $\blacksquare \in \mathbb{R}^{n+1}$ that defines it.

Lemma 4 (support of M_1)**.** *Let* $\blacksquare := [0..1]^{n+1}$ *and* $\mathbf{P}_{n+1} := \mathbf{I}_{n+1} - \mathbf{J}_{n+1}/(n+1)$*. The preimage of* $\overline{\mathrm{supp} M_1}$ *with respect to the map* $\mathbf{T}_1$ *decomposes into* $\ker \mathbf{T}_1 = \mathrm{span}(\mathbf{j})$ *and* $\mathbf{P}_{n+1}\blacksquare \subsetneq H_{\mathbf{j}}^n \subsetneq \mathbb{R}^{n+1}$*:*

$$\mathbf{T}_1^{-1}(\overline{\mathrm{supp} M_1}) = \mathbf{P}_{n+1}\blacksquare \oplus \mathrm{span}(\mathbf{j}).$$

Therefore $\mathbf{T}_1\blacksquare = \overline{\mathrm{supp} M_1} = \mathbf{T}_1\mathbf{P}_{n+1}\blacksquare$.

Proof. Recall that $\mathbf{A}_{\mathrm{P}}^*$ is composed of the first n columns of $\mathbf{P}_{n+1}$. By (24) and (8),

$$\mathbf{T}_1{}^t(\mathbf{T}_1\mathbf{T}_1{}^t)^{-1} = \frac{1}{n+1}\begin{bmatrix} (n+1)\mathbf{I}_n - \mathbf{J}_n \\ -\mathbf{j}^t \end{bmatrix} = \mathbf{A}_{\mathrm{P}}^* \in \mathbb{R}^{(n+1)\times n},$$

and therefore

$$\mathbf{T}_1{}^{-1}\{\boldsymbol{x}\} = \mathbf{A}_{\mathrm{P}}^*\boldsymbol{x} + \mathrm{span}(\mathbf{j}), \quad \boldsymbol{x} \in \mathbb{R}^n, \mathbf{j} \in \mathbb{R}^{n+1}. \tag{33}$$

By (15), $\overline{\mathrm{supp} M_1} = \mathbf{T}_1\blacksquare \subsetneq \mathbb{R}^n$ hence

$$\mathbf{T}_1{}^{-1}(\mathbf{T}_1\blacksquare) = \mathbf{A}_{\mathrm{P}}^*\mathbf{T}_1\blacksquare \oplus \mathrm{span}(\mathbf{j}) = \mathbf{P}_{n+1}\blacksquare \oplus \mathrm{span}(\mathbf{j}).$$

□

$\mathbf{P}_{n+1}\blacksquare$ is symmetric since the directions, i.e. the columns of $\mathbf{P}_{n+1}$, are isometric and isotropic. However, the domain embedded in the hyperplane $H_{\mathbf{j}}^n$ makes $M_{\mathbf{P}_{n+1}}$ difficult to use in applications. We therefore now introduce a square generator matrix $\mathbf{A}^*$ of $\mathcal{A}_n^*$.

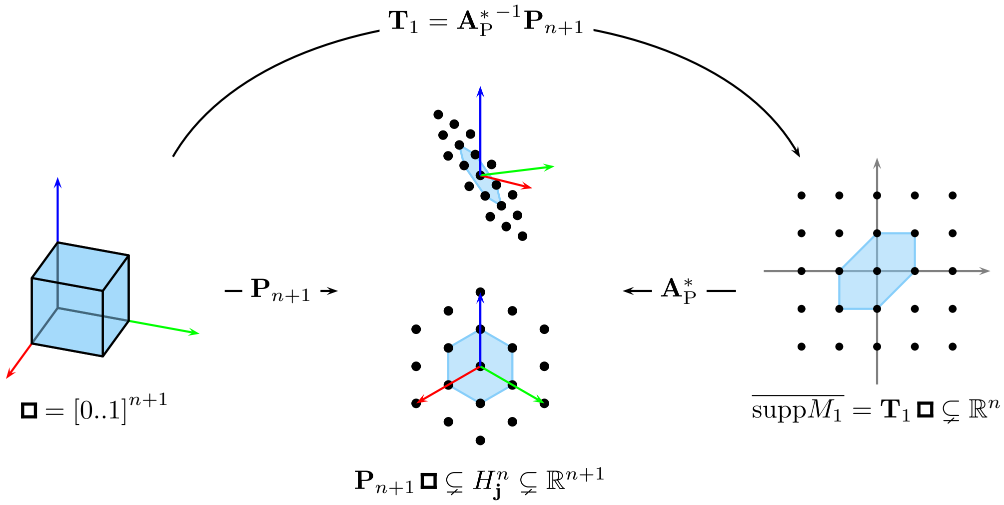

Figure 4: Symmetry of the support of $M_{\mathbf{P}_{n+1}}$ and asymmetry of the support of M_1.

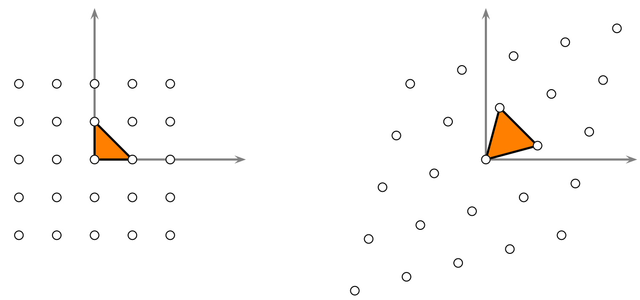

(a) $\mathbb{Z}^2$

(b) $\mathbf{A}{+}\mathbb{Z}^2 \cong \mathcal{A}_2$

Figure 5: Geometric construction of $\mathcal{A}_n$ in $\mathbb{R}^n$.

5.2. The new square generator matrices $\mathbf{A}$ *and* $\mathbf{A}^*$

To obtain a box-spline with a symmetric footprint in $\mathbb{R}^n$ (Figure 7(c) and 7(f)), we construct simple square generator matrices for $\mathcal{A}_n$ and $\mathcal{A}_n^*$. Consider a linear map that scales along the diagonal $\mathbf{j}$ by transforming a point $\boldsymbol{x} \in \mathbb{R}^n$ according to

$$\boldsymbol{x} \mapsto \boldsymbol{x} + \frac{c}{n}(\mathbf{j}\cdot\boldsymbol{x})\mathbf{j},$$

where c is the scaling factor.

Theorem 1 (Geometric construction of $\mathcal{A}_n$ (Figure 5) and $\mathcal{A}_n^*$ in $\mathbb{R}^n$ (Figure 6))**.**

(i) $\mathcal{A}_n$ *can be generated by*

$$\mathbf{A} := \mathbf{I}_n + \frac{c_n}{n}\mathbf{J}_n \quad \textit{with} \quad c_n := -1 \pm \sqrt{n+1}.$$

(ii) $\mathcal{A}_n^*$ *can be generated by*

$$\mathbf{A}^* := \mathbf{I}_n + \frac{c_n^*}{n}\mathbf{J}_n \quad \textit{with} \quad c_n^* = -1 \pm \frac{1}{\sqrt{n+1}}.$$

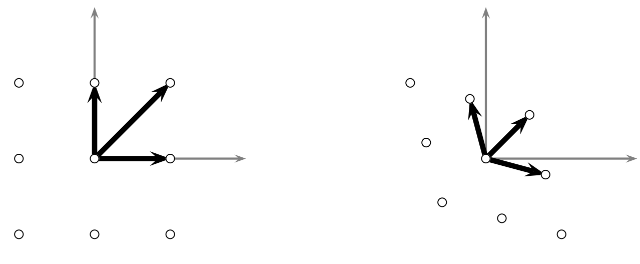

(a) $\mathbb{Z}^2$

(b) $\mathbf{A}^* + \mathbb{Z}^2 \cong \mathcal{A}_2^*$

Figure 6: Geometric construction of $\mathcal{A}_n^*$ in $\mathbb{R}^n$.

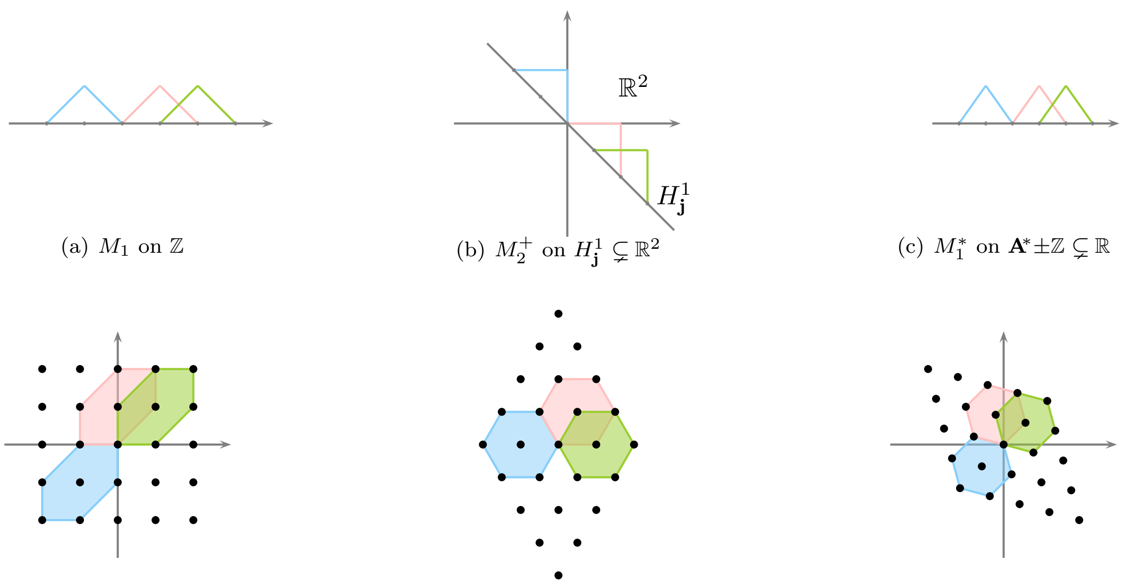

(a) M_1 on $\mathbb{Z}$

(b) M_2^+ on $H_{\mathbf{j}}^1 \subsetneq \mathbb{R}^2$

(c) M_1^* on $\mathbf{A}^* \pm \mathbb{Z} \subsetneq \mathbb{R}$

(d) M_1 on $\mathbb{Z}^2$

(e) M_3^+ on $H_{\mathbf{j}}^2 \subsetneq \mathbb{R}^3$

(f) M_1^* on $\mathbf{A}^* \pm \mathbb{Z}^2 \subsetneq \mathbb{R}^2$

Figure 7: (top) Shifts of linear univariate box-splines and (bottom) shifts of (the support) of linear bivariate box-splines.

Proof. (i) Any vector $\mathbf{i}_j - \mathbf{i}_k$ for $j \neq k$ is parallel to $H_{\mathbf{j}}^{n-1}$ and hence its length remains $\sqrt{2}$, unchanged by $\mathbf{A}$ and regardless of the dimension n. To show that the n-dimensional simplex $\mathrm{conv}(\{\mathbf{A}\mathbf{i}_j : 1 \leq j \leq n\} \cup \{\mathbf{0}\})$ is *equilateral*, we verify that the vectors $\mathbf{i}_j$ satisfy

$$\|\mathbf{A}\mathbf{i}_j\|_2 = \sqrt{\mathbf{A}\mathbf{i}_j \cdot \mathbf{A}\mathbf{i}_j} = \sqrt{\left(\frac{c_n}{n}+1\right)^2 + (n-1)\frac{{c_n}^2}{n^2}} = \sqrt{2}. \tag{34}$$

The claim follows by Lemma 2. The two different choices of c_n produce the equivalent result with respect to $H_{\mathbf{j}}^{n-1}$ because $\mathbf{I}_n - \mathbf{J}_n/n$ projects $\mathbf{i}_j$ on $H_{\mathbf{j}}^{n-1}$.

(ii) Since

$$1 = \left(\pm\sqrt{n+1}\right)\left(\pm\frac{1}{\sqrt{n+1}}\right) = (c_n+1)(c_n^*+1) = c_n c_n^* + c_n + c_n^* + 1,$$

$c_n c_n^* + c_n + c_n^* = 0$ and hence

$$\mathbf{A}^t\mathbf{A}^* = \mathbf{I}_n + (c_n c_n^* + c_n + c_n^*)\mathbf{J}_n = \mathbf{I}_n.$$

□

Under the diagonal scaling $\mathbf{A}^*$, the length of $\mathbf{j}$ becomes the same as those of the unit vectors (Figure 6):

$$|\mathbf{A}^*\mathbf{j}| = |\mathbf{A}^*\mathbf{i}_j|, \quad \forall 1 \leq j \leq n. \tag{35}$$

As with $\mathbf{A}$, two roots of c_n^* result in equivalent transformations with respect to $H_{\mathbf{j}}^{n-1}$. For example, for $n = 2$,

$$\mathbf{A}^* := \frac{1}{2}\begin{bmatrix} 1 \pm 1/\sqrt{3} & -1 \pm 1/\sqrt{3} \\ -1 \pm 1/\sqrt{3} & 1 \pm 1/\sqrt{3} \end{bmatrix}$$

and for $n = 3$, the BCC lattice, the two choices are

$$\mathbf{A}^* := \frac{1}{6}\begin{bmatrix} 5 & -1 & -1 \\ -1 & 5 & -1 \\ -1 & -1 & 5 \end{bmatrix} \quad \text{or} \quad \frac{1}{2}\begin{bmatrix} 1 & -1 & -1 \\ -1 & 1 & -1 \\ -1 & -1 & 1 \end{bmatrix}.$$

5.3. $\mathbf{A}^*\mathbb{Z}^n$ *as the domain lattice of* M_r^*

We now interpret the columns of the matrix $\mathbf{T}_r^* := \mathbf{A}^*\mathbf{T}_r$ as direction vectors in $\mathbb{R}^n$.

Lemma 5. $\mathbf{T}_1^*$ *is isometric and isotropic.*

Proof. Since (35) implies isometry, we need only verify isotropy,

$$(\mathbf{A}^*(-\mathbf{j}))\cdot(\mathbf{A}^*\mathbf{i}_j) = -\frac{1}{n+1}, \quad \forall \mathbf{i}_j \quad \text{and} \quad (\mathbf{A}^*\mathbf{i}_k)\cdot(\mathbf{A}^*\mathbf{i}_j) = -\frac{1}{n+1}, \quad \forall \mathbf{i}_j \neq \mathbf{i}_k.$$

□

Therefore $M_{\mathbf{T}_r^*}$ has the same symmetries as $\mathcal{A}_n^*$ and $\mathbf{A}^*\mathbb{Z}^n \cong \mathcal{A}_n^*$ can serve as a domain lattice for the box-spline family (Figure 7(c) and 7(f))

$$M_r^* := |\det \mathbf{A}^*| M_{\mathbf{T}_r^*} = M_r \circ {\mathbf{A}^*}^{-1}. \tag{36}$$

Since, in contrast to (33), for M_1

$$(\mathbf{A}_{\mathrm{P}}^*{\mathbf{A}^*}^{-1})^t(\mathbf{A}_{\mathrm{P}}^*{\mathbf{A}^*}^{-1}) = \mathbf{I}_n,$$

the symmetry of $\mathbf{P}_{n+1}\boxdot$ is preserved when computing the preimage,

$${\mathbf{T}_1^*}^{-1}\{\boldsymbol{x}\} = \mathbf{A}_{\mathrm{P}}^*{\mathbf{A}^*}^{-1}\{\boldsymbol{x}\} + \ker \mathbf{T}_1^*. \tag{37}$$

6. The Symmetric Box-spline Family M_r^* on $\mathbf{A}^*\mathbb{Z}^n$

By (27), the weighted sum of the shifts of M_r^* on $\mathbf{A}^*\mathbb{Z}^n \cong \mathcal{A}_n^*$ can be expressed as

$$\sum_{\boldsymbol{j}\in\mathbf{A}^*\mathbb{Z}^n} M_r^*\,(\cdot-\boldsymbol{j})\,a(\boldsymbol{j}) = \sum_{\boldsymbol{j}\in\mathbb{Z}^n} M_r(\mathbf{A}^{*-1}\cdot-\boldsymbol{j})a(\mathbf{A}^*j). \tag{38}$$

Therefore M_r^* inherits most of the properties of M_r. In particular, by (10), M_r, hence M_r^*, is a piecewise polynomial of (total) degree less than or equal to $(n+1)r-n$. We now summarize its properties (and those of its scaled copy $M_{\mathbf{T}_r^*}$, cf. (36))

Theorem 2 (Properties of M_r^*)**.** *The box-spline M_r^* has the following properties:*

(i) M_r^* is centered.

(ii) $M_{\mathbf{T}_r^*} = M_{-\mathbf{T}_r^*}$

(iii) $M_r^* = M_r^*(-\cdot)$ is an even function.

(iv) The sequence $(M_r^*(\cdot-\boldsymbol{j}))_{\boldsymbol{j}\in\mathbf{A}^*\mathbb{Z}^n}$ is linearly independent.

(v) The map $M_r^* *'$ (19) can reproduce all the polynomials of (total) degree up to $2r-1$:

$$m(\mathbf{T}_r^*) = 2r-1.$$

Proof. (i) By (11),

$$M_r^{*c} := M_r^*\left(\cdot+\frac{1}{2}\sum_{\boldsymbol{\xi}\in\mathbf{T}_r^*}\boldsymbol{\xi}\right) = M_r^* \tag{39}$$

since $\sum_{\boldsymbol{\xi}\in\mathbf{T}_r^*}\boldsymbol{\xi} = \mathbf{0}$.

(ii) By (14),

$$\mathcal{F}\left\{M_{\mathbf{T}_r^*}\right\}(\boldsymbol{\omega}) = \prod_{\boldsymbol{\xi}\in\mathbf{T}_r^*}\operatorname{sinc}(\boldsymbol{\xi}\cdot\boldsymbol{\omega})$$

and

$$\mathcal{F}\left\{M_{-\mathbf{T}_r^*}\right\}(\boldsymbol{\omega}) = \prod_{\boldsymbol{\xi}\in-\mathbf{T}_r^*}\operatorname{sinc}(\boldsymbol{\xi}\cdot\boldsymbol{\omega}) = \prod_{\boldsymbol{\xi}\in\mathbf{T}_r^*}\operatorname{sinc}(-\boldsymbol{\xi}\cdot\boldsymbol{\omega}) = \prod_{\boldsymbol{\xi}\in\mathbf{T}_r^*}\operatorname{sinc}(\boldsymbol{\xi}\cdot\boldsymbol{\omega})$$

because sinc is an even function. The claim holds since the Fourier transform is invertible.

(iii) By (12) and (i),

$$M_{\mathbf{T}_r^*} = |\det(-\mathbf{I}_n)|M_{-\mathbf{T}_r^*}\circ(-\mathbf{I}_n) = M_{\mathbf{T}_r^*}(-\cdot). \tag{40}$$

(iv) Since any n directions in $\mathbf{T}_1$ span $\mathbb{R}^n$,

$$\det\mathbf{Z} = \pm1,\quad \forall\mathbf{Z}\in\bigcup_{\boldsymbol{\xi}\in\mathbf{T}_1}\mathbf{T}_1\backslash\{\boldsymbol{\xi}\} = \mathcal{B}(\mathbf{T}_1) = \mathcal{B}(\mathbf{T}_r)$$

and the sequence $(M_r(\cdot-\boldsymbol{j}))_{\boldsymbol{j}\in\mathbb{Z}^n}$ is linearly independent. claim (iv) follows since by (38), the shifts of M_r on the integer grid and the shifts of M_r^* on $\mathbf{A}^*\mathbb{Z}^n$ are related by an invertible affine change of variables.

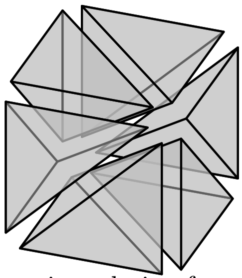

Figure 8: Kuhn triangulation for $n = 3$.

(v) Due to (38), $m(\mathbf{T}_r^*) = m(\mathbf{T}_r)$. For M_1, we have to remove at least 2 directions so that the remaining directions in $\mathbf{T}_1$ no longer span $\mathbb{R}^n$, hence

$$m(\mathbf{T}_1) = ((n+1) - (n-1)) - 1 = 2 - 1 = 1.$$

In the same way, at most $r(n-1)$ directions in $\mathbf{T}_r$ span a hyperplane, therefore

$$m(\mathbf{T}_r) = (r(n+1) - r(n-1)) - 1 = 2r - 1.$$

$\square$

Note that $m(\mathbf{T}_r^*)$ does not depend on the dimension n.

Next, we characterize the partition of $\mathbb{R}^n$ induced by the knot planes in $\mathbb{H}(\mathbf{T}_r)$. Since the knot planes generated by $\mathbf{T}_r^*$ are those of $\Gamma(\mathbf{T}_r)$ under invertible linear transformation, the mesh inherits the topology of the $(n+1)$-directional mesh.

Lemma 6 (Partition by knot planes)**.**
(i) There are $n(n+1)/2$ non-parallel planes in $\mathbb{H}(\mathbf{T}_r)$.
(ii) The knot planes in $\mathbb{H}(\mathbf{T}_r)$ partition the unit cube $\square$ into $n!$ simplices (Figure 8)

$$\sigma_\pi := \operatorname{conv}(V_\pi), \quad V_\pi := \{\mathbf{0}\} \cup \bigcup_{i=1}^{n} \sum_{j=1}^{i} \{\mathbf{i}_{\pi(j)}\}, \quad \pi \in S_n \tag{41}$$

where S_n be the set of all the permutations of $\{1, \cdots, n\}$.

The partition $\{\sigma_\pi\}_{\pi \in S_n}$ is called *Freudenthal triangulation* [20] or *Kuhn triangulation.*

Proof. (i) There are n planes generated by the n unit vectors in $\mathbf{I}_n$ and $\binom{n}{n-2}$ additional non-parallel planes are spanned by the diagonal direction $\mathbf{j}$ and $n-2$ additional unit vectors yielding a total of

$$n + \binom{n}{n-2} = n + \frac{1}{2}n(n-1) = \frac{1}{2}n(n+1)$$

non-parallel planes in $\mathbb{H}(\mathbf{T}_r)$.

(ii) Recall that $T_1 = \begin{bmatrix}\mathbf{I}_n & -\mathbf{j}\end{bmatrix}$. All planes with normal direction $\mathbf{i}_j - \mathbf{i}_k$, $j \neq k$, intersect the interior of $\square$ and are generated by $\mathbf{T}_1 \backslash \{\mathbf{i}_j, \mathbf{i}_k\}$ i.e., as knot planes of M_1 generated by $n-1$ vectors including $\mathbf{j}$. Unless two vertices $\boldsymbol{v}_j, \boldsymbol{v}_k$ are both in V_π for some permutation π, there exist indices α and β so that

$$\boldsymbol{v}_j(\alpha) = 1, \boldsymbol{v}_k(\alpha) = 0 \quad \text{and} \quad \boldsymbol{v}_j(\beta) = 0, \boldsymbol{v}_k(\beta) = 1$$

and hence the knot plane with normal $\mathbf{i}_\alpha - \mathbf{i}_\beta$ separates them,

$$(\mathbf{i}_\alpha - \mathbf{i}_\beta) \cdot \boldsymbol{v}_j = 1 > 0 \quad \text{and} \quad (\mathbf{i}_\alpha - \mathbf{i}_\beta) \cdot \boldsymbol{v}_k = -1 < 0. \tag{42}$$

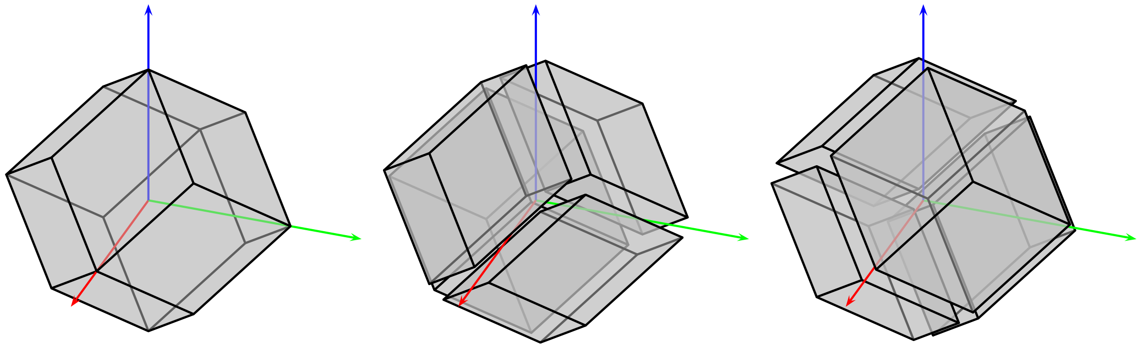

(a) (b) (c)

Figure 9: (a) Rhombic dodecahedron: support of M_1^* for $n = 3$ and $\mathbf{A}^* = \frac{1}{2}\begin{bmatrix} 1 & -1 & -1 \\ -1 & 1 & -1 \\ -1 & -1 & 1 \end{bmatrix}$. Figures (b)(c): two decomposition of the support into parallelepipeds: (b) by (43) and (c) by (44).

Conversely, since knot planes excluding $\mathbf{j}$ are axis-aligned, neither they nor their shifts on $\mathbb{Z}^n$ intersect the interior of the unit cube $\square$. It remains to show that no shifts of the knot planes with normal $\mathbf{i}_\alpha - \mathbf{i}_\beta$ separate vertices of a simplex σ_π for the same fixed permutation π. Since $\boldsymbol{j} \cdot (\mathbf{i}_\alpha - \mathbf{i}_\beta) = \boldsymbol{j}(\alpha) - \boldsymbol{j}(\beta) = 0$, any shifts by $\boldsymbol{j} \in \mathbb{Z}^n$ within the knot plane $\{\boldsymbol{x} \in \mathbb{R}^n : (\mathbf{i}_\alpha - \mathbf{i}_\beta) \cdot \boldsymbol{x} = 0\}$ result in the same plane $\{\boldsymbol{x} \in \mathbb{R}^n : (\mathbf{i}_\alpha - \mathbf{i}_\beta) \cdot (\boldsymbol{x} - \boldsymbol{j}) = 0\}$ and therefore we can assume that $\boldsymbol{j} \cdot (\mathbf{i}_\alpha - \mathbf{i}_\beta) = \boldsymbol{j}(\alpha) - \boldsymbol{j}(\beta) > 0$. Then, for all $\boldsymbol{v} \in \{0, 1\}^n$,

$$(\mathbf{i}_\alpha - \mathbf{i}_\beta) \cdot (\boldsymbol{v} - \boldsymbol{j}) = \begin{cases} -\boldsymbol{j}(\alpha) + \boldsymbol{j}(\beta) + 1 <= 0 & \boldsymbol{v}(\alpha) = 1, \boldsymbol{v}(\beta) = 0 \\ -\boldsymbol{j}(\alpha) + \boldsymbol{j}(\beta) - 1 < -1 & \boldsymbol{v}(\alpha) = 0, \boldsymbol{v}(\beta) = 1 \\ -\boldsymbol{j}(\alpha) + \boldsymbol{j}(\beta) < 0 & \boldsymbol{v}(\alpha) = \boldsymbol{v}(\beta) \end{cases}$$
$$\leq 0.$$

The case $\boldsymbol{j} \cdot (\mathbf{i}_\alpha - \mathbf{i}_\beta) < 0$ corresponds to a flipped normal and yields $(\mathbf{i}_\alpha - \mathbf{i}_\beta) \cdot (\boldsymbol{v} - \boldsymbol{j}) \geq 0$. □

With the help of Lemma 6, we can establish the structure of suppM_r^* by first decomposing it into parallelepipeds. There are two decompositions (see Figure 9).

Theorem 3 (support of M_1^*)**.** *The (closed) support of M_1^* is the essentially disjoint union of the $(n+1)$ parallelepipeds*

$$\{\mathbf{Z}\square : \mathbf{Z} \in \mathcal{B}(\mathbf{T}_1^*)\} \tag{43}$$

or, alternatively,

$$\{\mathbf{Z}\square + \zeta_{\mathbf{Z}} : \mathbf{Z} \in \mathcal{B}(\mathbf{T}_1^*)\} \tag{44}$$

where $\zeta_{\mathbf{Z}} := \mathbf{T}_1^* \backslash \mathbf{Z}$. In either decomposition, all the parallelepipeds are congruent.

Proof. Due to the relation (38), we need only consider M_1. Let $\mathbf{Z}_j \in \mathcal{B}(\mathbf{T}_1)$ be a basis of $\mathbf{T}_1$ and

$$\boldsymbol{\zeta}_j := \mathbf{T}_1 \backslash \mathbf{Z}_j = -\sum_{\boldsymbol{\xi} \in \mathbf{Z}_j} \boldsymbol{\xi}.$$

For $\boldsymbol{\alpha}_j := \boldsymbol{\alpha}_{\mathbf{Z}_j}$ in (17), there are only two choices, $\boldsymbol{\alpha}_j \in \{\mathbf{0}, \boldsymbol{\zeta}_j\}$, since for any $\boldsymbol{\zeta} \in \mathbf{Z}_j$, $2\boldsymbol{\zeta}$ does not fit into $\mathbf{T}_1\square$ (cf. Figure 4, *right*):

$$\forall \boldsymbol{\zeta} \in \mathbf{Z}_j, \qquad \boldsymbol{\zeta} + \boldsymbol{\zeta} \in \mathbf{Z}_j\square + \boldsymbol{\zeta} \quad \text{but} \quad \boldsymbol{\zeta} + \boldsymbol{\zeta} \notin \quad \mathbf{T}_1\square.$$

Now assume

$$\boldsymbol{\alpha}_j = \mathbf{0} \quad \text{and} \quad \boldsymbol{\alpha}_k = \boldsymbol{\zeta}_k \quad \text{for } \mathbf{Z}_j, \mathbf{Z}_k \in \mathcal{B}(\mathbf{T}_1), \mathbf{Z}_j \neq \mathbf{Z}_k.$$

This leads to a contradiction as we prove that the two parallelepipeds $\mathbf{Z}_j \square + \boldsymbol{\alpha}_j$ and $\mathbf{Z}_k \square + \boldsymbol{\alpha}_k$ are not essentially disjoint but rather share the point

$$\boldsymbol{p} := \frac{1}{2}\boldsymbol{\zeta}_k + \frac{1}{4} \sum_{\boldsymbol{\zeta} \in \mathbf{Z}_j \cap \mathbf{Z}_k} \boldsymbol{\zeta}.$$

To verify that $\boldsymbol{p}$ is in the interior of both parallelepipeds, let $\oplus$ denote the disjoint union and observe that $\mathbf{Z}_j = (\mathbf{Z}_j \backslash \mathbf{Z}_k) \oplus (\mathbf{Z}_j \cap \mathbf{Z}_k)$ and $\{\boldsymbol{\zeta}_k\} = \mathbf{T}_1 \backslash \mathbf{Z}_k = \mathbf{Z}_j \backslash \mathbf{Z}_k$ so that for $\boldsymbol{\alpha}_j = \mathbf{0}$,

$$\boldsymbol{p} = \left(\frac{1}{2} \sum_{\boldsymbol{\zeta} \in \mathbf{Z}_j \backslash \mathbf{Z}_k} \boldsymbol{\zeta} + \frac{1}{4} \sum_{\boldsymbol{\zeta} \in \mathbf{Z}_j \cap \mathbf{Z}_k} \boldsymbol{\zeta} \right) + \boldsymbol{\alpha}_j.$$

That is, $\boldsymbol{p} \in \mathbf{Z}_j(0,1)^n + \boldsymbol{\alpha}_j$. (We use $(0,1)^n$ rather than $\square$ to show essential disjointedness).
But also $\boldsymbol{p} \in \mathbf{Z}_k(0,1)^n + \boldsymbol{\alpha}_k$ since

$$\begin{aligned}
\boldsymbol{p} &= \frac{1}{2}\boldsymbol{\zeta}_k + \frac{1}{4} \sum_{\boldsymbol{\zeta} \in \mathbf{Z}_j \cap \mathbf{Z}_k} \boldsymbol{\zeta} + \frac{1}{2} \sum_{\boldsymbol{\zeta} \in \mathbf{T}_1} \boldsymbol{\zeta} && \left(\textstyle\sum_{\boldsymbol{\zeta} \in \mathbf{T}_1} \boldsymbol{\zeta} = \mathbf{0}\right) \\
&= \frac{1}{2}\boldsymbol{\zeta}_k + \frac{1}{4} \sum_{\boldsymbol{\zeta} \in \mathbf{Z}_j \cap \mathbf{Z}_k} \boldsymbol{\zeta} + \frac{1}{2} \sum_{\boldsymbol{\zeta} \in \mathbf{Z}_k} \boldsymbol{\zeta} + \frac{1}{2}\boldsymbol{\zeta}_k \\
&= \left(\frac{3}{4} \sum_{\boldsymbol{\zeta} \in \mathbf{Z}_j \cap \mathbf{Z}_k} \boldsymbol{\zeta} + \frac{1}{2} \sum_{\boldsymbol{\zeta} \in \mathbf{Z}_k \backslash \mathbf{Z}_j} \boldsymbol{\zeta} \right) + \boldsymbol{\alpha}_k.
\end{aligned}$$

This establishes that there are only the two listed alternatives.

Next, we prove that all parallelepipeds are congruent. To analyze the decomposition

$$\{\mathbf{Z}^* \square : \mathbf{Z}^* \in \mathcal{B}(\mathbf{T}_1^*)\} \tag{45}$$

we observe that

- the matrices $\mathbf{X}_\alpha, \mathbf{Y}_\alpha \in \mathbb{R}^{n \times n}$

$$\mathbf{X}_\alpha(j,k) := \begin{cases} 1 & k = \alpha \\ 0 & \text{otherwise} \end{cases} \quad \text{and} \quad \mathbf{Y}_\alpha(j,k) := \begin{cases} 1 & j = k = \alpha \\ 0 & \text{otherwise} \end{cases}$$

  satisfy the relations

$$\mathbf{X}_j \mathbf{J}_n = \mathbf{J}_n,\ \mathbf{Y}_j \mathbf{J}_n = \mathbf{X}_j^t,\ \mathbf{X}_j \mathbf{X}_j^t = \mathbf{J}_n,\ \mathbf{X}_j \mathbf{Y}_j = \mathbf{X}_j,\ \mathbf{Y}_j \mathbf{X}_j = \mathbf{Y}_j,\ \mathbf{X}_j^2 = \mathbf{X}_j$$

  and that

- for $\mathbf{Z}_j := \mathbf{I}_n - \mathbf{X}_j - \mathbf{Y}_j$,

$$\mathbf{Z}_j(\mathbf{I}_n + \mathbf{J}_n)\mathbf{Z}_j^t = \mathbf{I}_n + \mathbf{J}_n \text{ and } \mathbf{Z}_j^2 = \mathbf{I}_n.$$

  Then since $\mathbf{A}^2 = \mathbf{I}_n + \mathbf{J}_n$, for $\mathbf{Z}_j^* := \mathbf{A}^* \mathbf{Z}_j$ and $\mathbf{Z}_k^* := \mathbf{A}^* \mathbf{Z}_k$,

$$\mathbf{Z}_j^* = (\mathbf{A}^* \mathbf{Z}_j \mathbf{Z}_k \mathbf{A}^{*-1}) \mathbf{Z}_k^*. \tag{46}$$

Secondly, we verify that

$$
\begin{aligned}
(\mathbf{A}^*\mathbf{Z}_j\mathbf{Z}_k{\mathbf{A}^*}^{-1})(\mathbf{A}^*\mathbf{Z}_j\mathbf{Z}_k{\mathbf{A}^*}^{-1})^t &= \mathbf{A}^*\mathbf{Z}_j\mathbf{Z}_k\mathbf{A}^2\mathbf{Z}_k^t\mathbf{Z}_j^t\mathbf{A}^* && ({\mathbf{A}^*}^{-1} = \mathbf{A}) \\
&= \mathbf{A}^*(\mathbf{I}_n + \mathbf{J}_n)\mathbf{A}^* && (46) \\
&= \mathbf{I}_n.
\end{aligned}
$$

For $\mathbf{A}^*\mathbf{Z}_j, \mathbf{A}^*\mathbf{Z}_k \in \mathcal{B}(\mathbf{T}_1^*)$, $\mathbf{A}^*\mathbf{Z}_j\mathbf{Z}_k{\mathbf{A}^*}^{-1}$ is therefore an orthonormal (rigid) transformation. And hence, by (46), all the parallelepipeds $\mathbf{Z}^*\,\square$, for $\mathbf{Z}^* \in \mathcal{B}(\mathbf{T}_1^*)$ are congruent. The other decomposition is verified in the same way. □

Lemma 3 is easily extended to $\mathbf{T}_r^*$ since

$$\mathbf{T}_r^*\,\square = \{\sum_{\boldsymbol{\xi}\in\mathbf{T}_r^*} \boldsymbol{\xi} \boldsymbol{t}_{\boldsymbol{\xi}} : 0 \le \boldsymbol{t}_{\boldsymbol{\xi}} \le 1\} = \{\sum_{\boldsymbol{\xi}\in\mathbf{T}_1^*} \boldsymbol{\xi} \boldsymbol{t}_{\boldsymbol{\xi}} : 0 \le \boldsymbol{t}_{\boldsymbol{\xi}} \le r\} = \mathbf{T}_1^*(r\,\square).$$

For $\mathbf{Z} \in \mathcal{B}(\mathbf{T}_1^*)$, the pair $(\mathbf{Z}, \zeta_{\mathbf{Z}})$ is a linear transformation of the pair $(\mathbf{I}_n, -\mathbf{j})$. Therefore $\mathbf{Z}\,\square$ is decomposed in the same way as the unit cube $\square$ is decomposed by the Kuhn triangulation and suppM_1^* consists of $n!$ simplices. This count also agrees with the number of *modular cells* in the first neighbor polytope of $\mathcal{A}_n^*$ [21]. The two types of the decomposition of suppM_1^* in Lemma 3 can be viewed as cubical meshes such that one is the *flip* of the other [3] since each cubical mesh can be viewed as the projection of the $(n+1)$-dimensional cube along one fixed diagonal in two opposite directions.

Next, we expand on Theorem 2(v), which showed that M_2^* can reproduce all cubic polynomials. The following lemma will simplify the proof.

Lemma 7. *For an odd function f, $\mu_{\mathbf{T}_2} f = 0$.*

Proof. By definition (22),

$$
\begin{aligned}
\mu_{\mathbf{T}_2} f &= \sum_{\boldsymbol{j}} M_2(-\boldsymbol{j}) f(\boldsymbol{j}) \\
&= \sum_{\boldsymbol{j}} M_2(\boldsymbol{j}) f(\boldsymbol{j}) && \text{(by Thm (2)(iii))} \\
&= -\sum_{\boldsymbol{j}} M_2(\boldsymbol{j}) f(-\boldsymbol{j}) && (f = -f(-\cdot)) \\
&= -\sum_{\boldsymbol{j}} M_2(-\boldsymbol{j}) f(\boldsymbol{j}). && \text{(change of index)}
\end{aligned}
$$

Comparing the first to the fourth line, we see $\mu_{\mathbf{T}_2} f = 0$. □

Theorem 4 (Quasi-interpolant for M_2^*)**.** *The quasi-interpolant of M_2^*, defined by the functional*

$$\lambda_2^*(f(\cdot + j)) := \lambda_{\mathbf{T}_2}^{\mathbf{A}^*}(f(\cdot + \boldsymbol{j})) := \left(f - \frac{1}{12} \sum_{\boldsymbol{\xi}\in\mathbf{T}_1^*} D_{\boldsymbol{\xi}}^2 f \right)(\boldsymbol{j}), \quad j \in \mathbf{A}^*\mathbb{Z}^n \tag{47}$$

provides the maximal approximation power $m(\mathbf{T}_2) + 1 = 4$.

Proof. We derive the quasi-interpolant $Q_{\mathbf{T}_2}$ for $S_{\mathbf{T}_2}$ defined by $\lambda_{\mathbf{T}_2}$ (21). Then $Q_{\mathbf{T}_2}^{\mathbf{A}^*}$ for $S_{\mathbf{T}_2}^{\mathbf{A}^*}$ defined by λ_2^* can be derived by (28).

Specifically, we compute $g_{\boldsymbol{\alpha}}(\mathbf{0})$ for each degree $|\boldsymbol{\alpha}|$.

1. $|\boldsymbol{\alpha}| = 0$

   $g_{\boldsymbol{\alpha}}(\mathbf{0}) = g_{\mathbf{0}}(\mathbf{0}) = 1$ By [13, page 68].

2. $|\boldsymbol{\alpha}| = 1$

   By Lemma 7, $\mu_{\mathbf{T}_2}[\![]\!]^{\boldsymbol{\alpha}} = 0$ and

$$g_{\boldsymbol{\alpha}} = [\![]\!]^{\boldsymbol{\alpha}} - \sum_{\boldsymbol{\beta}\neq\boldsymbol{\alpha}} \left(\mu_{\mathbf{T}_2}[\![]\!]^{\boldsymbol{\alpha}-\boldsymbol{\beta}}\right) g_{\boldsymbol{\beta}} = [\![]\!]^{\boldsymbol{\alpha}} - \left(\mu_{\mathbf{T}_2}[\![]\!]^{\boldsymbol{\alpha}}\right) g_{\mathbf{0}} = [\![]\!]^{\boldsymbol{\alpha}}$$

   therefore $g_{\boldsymbol{\alpha}}(\mathbf{0}) = 0$.

3. $|\boldsymbol{\alpha}| = 2$

   By [13, page 11],

$$\widehat{M}_{\mathbf{T}_2}(\boldsymbol{\omega}) := \mathcal{F}\left\{M_{\mathbf{T}_2}\right\}(\boldsymbol{\omega}) = \prod_{\boldsymbol{\xi}\in\mathbf{T}_2} \operatorname{sinc}(\boldsymbol{\xi}\cdot\boldsymbol{\omega}) = \prod_{\boldsymbol{\xi}\in\mathbf{T}_1} \operatorname{sinc}^2(\boldsymbol{\xi}\cdot\boldsymbol{\omega}).$$

   Therefore, By (23), for $j \neq k$,

$$\begin{aligned}&\left(D_j D_k \frac{1}{\widehat{M}_{\mathbf{T}_2}}\right)(\boldsymbol{\omega}) \\ &= \left(\prod_{\boldsymbol{\xi}\in\mathbf{T}_1\setminus\{\mathbf{j},\mathbf{i}_j,\mathbf{i}_k\}} \frac{1}{\operatorname{sinc}^2(\boldsymbol{\xi}\cdot\boldsymbol{\omega})}\right) D_j D_k \frac{1}{\operatorname{sinc}^2(\mathbf{j}\cdot\boldsymbol{\omega})\operatorname{sinc}^2(\boldsymbol{\omega}_j)\operatorname{sinc}^2(\boldsymbol{\omega}_k)}\end{aligned}$$

   Since $\operatorname{sinc}(\mathbf{0}) = 1$, with the help of `MAPLE`, we can compute

$$\left(D_j D_k \frac{1}{\widehat{M}_{\mathbf{T}_2}}\right)(\mathbf{0}) = \left(D_j D_k \frac{1}{\operatorname{sinc}^2(\boldsymbol{\omega}_j)\operatorname{sinc}^2(\boldsymbol{\omega}_j)\operatorname{sinc}^2(\boldsymbol{\omega}_j+\boldsymbol{\omega}_k)}\right)(\mathbf{0}) = \frac{1}{6}.$$

   Also,

$$\left(D_j^2 \frac{1}{\widehat{M}_{\mathbf{T}_2}}\right)(\boldsymbol{\omega}) = \left(\prod_{\boldsymbol{\xi}\in\mathbf{T}_1\setminus\{\mathbf{j},\mathbf{i}_j\}} \frac{1}{\operatorname{sinc}^2(\boldsymbol{\xi}\cdot\boldsymbol{\omega})}\right) D_j^2 \frac{1}{\operatorname{sinc}^2(\mathbf{j}\cdot\boldsymbol{\omega})\operatorname{sinc}^2(\boldsymbol{\omega}_j)}.$$

   Again, with the help of `MAPLE`, we can compute

$$\left(D_j^2 \frac{1}{\widehat{M}_{\mathbf{T}_2}}\right)(\mathbf{0}) = \left(D_j^2 \frac{1}{\operatorname{sinc}^4(\boldsymbol{\omega}_j)}\right)(\mathbf{0}) = \frac{1}{3}.$$

   By (23), for $j \neq k$,

$$g_{\mathbf{i}_j+\mathbf{i}_k}(\mathbf{0}) = \left([\![-iD]\!]^{\mathbf{i}_j+\mathbf{i}_k} \frac{1}{\widehat{M}_{\mathbf{T}_2}}\right)(\mathbf{0}) = \left(-D_j D_k \frac{1}{\widehat{M}_{\mathbf{T}_2}}\right)(\mathbf{0}) = -\frac{1}{6}$$

   and

$$g_{2\mathbf{i}_j}(\mathbf{0}) = \left([\![-iD]\!]^{2\mathbf{i}_j} \frac{1}{\widehat{M}_{\mathbf{T}_2}}\right)(\mathbf{0}) = \left(-\frac{1}{2}D_j^2 \frac{1}{\widehat{M}_{\mathbf{T}_2}}\right)(\mathbf{0}) = -\frac{1}{6}.$$

4. $|\boldsymbol{\alpha}| = 3$

   By [13, (III.19)],

$$
\begin{aligned}
g_{\boldsymbol{\alpha}} &= [\![]\!]^{\boldsymbol{\alpha}} - \sum_{\boldsymbol{\beta}\neq\boldsymbol{\alpha}} \left(\mu_{\mathbf{T}_2} [\![]\!]^{\boldsymbol{\alpha}-\boldsymbol{\beta}}\right) g_{\boldsymbol{\beta}} \\
&= [\![]\!]^{\boldsymbol{\alpha}} - \left(\left(\mu_{\mathbf{T}_2} [\![]\!]^{\boldsymbol{\alpha}}\right) g_{\mathbf{0}} + \sum_{|\boldsymbol{\beta}|=1} \left(\mu_{\mathbf{T}_2} [\![]\!]^{\boldsymbol{\alpha}-\boldsymbol{\beta}}\right) g_{\boldsymbol{\beta}} + \sum_{|\boldsymbol{\beta}|=2} \left(\mu_{\mathbf{T}_2} [\![]\!]^{\boldsymbol{\alpha}-\boldsymbol{\beta}}\right) g_{\boldsymbol{\beta}} \right) \\
&= [\![]\!]^{\boldsymbol{\alpha}}
\end{aligned}
$$

   hence $g_{\boldsymbol{\alpha}}(\mathbf{0}) = 0$ because

   - $\mu_{\mathbf{T}_2} [\![]\!]^{\boldsymbol{\alpha}} = 0$ by Lemma 7,
   - $g_{\boldsymbol{\beta}} = 0$ for $|\boldsymbol{\beta}| = 1$ and
   - $\mu_{\mathbf{T}_2} [\![]\!]^{\boldsymbol{\alpha}-\boldsymbol{\beta}} = 0$ for $|\boldsymbol{\beta}| = 2$ hence $|\boldsymbol{\alpha} - \boldsymbol{\beta}| = 1$ by Lemma 7.

Summing up,

$$
\begin{aligned}
\lambda_{\mathbf{T}_2} f &= \sum_{|\boldsymbol{\alpha}|\leq m(\mathbf{T}_2)} g_{\boldsymbol{\alpha}}(\mathbf{0}) \left(D^{\boldsymbol{\alpha}} f\right)(\mathbf{0}) \\
&= f(\mathbf{0}) - \frac{1}{6} \sum_{|\boldsymbol{\alpha}|=2} (D^{\boldsymbol{\alpha}} f)(\mathbf{0}) \\
&= f(\mathbf{0}) - \frac{1}{12} \left(\sum_{k=1}^{n} (D_k^2 f)(\mathbf{0}) + ((\sum_{k=1}^{n} D_k)^2 f)(\mathbf{0}) \right) \\
&= f(\mathbf{0}) - \frac{1}{12} \sum_{\boldsymbol{\xi}\in\mathbf{T}_1} (D_{\boldsymbol{\xi}}^2 f)(\mathbf{0}). \qquad (48)
\end{aligned}
$$

Now, by (29),

$$
\lambda_2^* f = f(\mathbf{0}) - \frac{1}{12} \sum_{\boldsymbol{\xi}\in\mathbf{T}_1^*} (D_{\boldsymbol{\xi}}^2 f)(\mathbf{0}).
$$

□

For discrete input $f : \mathbf{A}^*\mathbb{Z}^n \to \mathbb{R}$, we approximate the directional derivative along $\zeta \in \mathbb{R}^n$ by finite differences, e.g.,

$$
D_\zeta^2 f \approx f(\cdot + \zeta) + f(\cdot - \zeta) - 2f. \qquad (49)
$$

Therefore

$$
\begin{aligned}
\lambda_2^* f &\approx f(\mathbf{0}) - \frac{1}{12} \sum_{\boldsymbol{\xi}\in\mathbf{T}_1^*} \left(f(\boldsymbol{\xi}) + f(-\boldsymbol{\xi}) - 2f(\mathbf{0})\right) \\
&= \left(1 + \frac{n+1}{6}\right) f(\mathbf{0}) - \frac{1}{12} \sum_{\boldsymbol{\xi}\in\mathbf{T}_1^*} \left(f(\boldsymbol{\xi}) + f(-\boldsymbol{\xi})\right). \qquad (50)
\end{aligned}
$$

When specialized to two variables, this agrees with Levin's formula [27].

7. Conclusion

We introduced a non-standard representation $\mathbf{A}^*\mathbb{Z}^n$ of the efficient reconstruction lattice $\mathcal{A}_n^*$ that is based on a new family of square generator matrices $\mathbf{A}^*$. In this representation, $\mathcal{A}_n^*$ naturally admits a *symmetric* box-spline family M_r^*. We then documented, in any number of variables n, the support, the induced partition of $\mathbb{R}^n$ and the desirable properties shared with the well-known box-spline family M_r. For the important case $r = 2$ that provides a smooth field of low degree, we derived in any number of variables an optimal quasi-interpolant construction for M_2^*.

8. Acknowledgment

This work was supported in part by NSF Grant CCF-0728797.

References

[1] E. Arge and M. Dæhlen. Grid point interpolation on finite regions using C^1 box splines. *SIAM Journal of Numerical Analysis*, 29(4):1136–1153, 1992.

[2] A. Bejancu. Semi-cardinal interpolation and difference equations: From cubic B-splines to a three-direction box-spline construction. *Journal of Computational and Applied Mathematics*, 197(1):62–77, December 2006.

[3] M. W. Bern, D. Eppstein, and J. G. Erickson. Flipping cubical meshes. *Engineering with Computers*, 18(3):173–187, October 2002.

[4] G. Casciola, E. Franchini, and L. Romani. The mixed directional difference-summation algorithm for generating the Bézier net of a trivariate four-direction box-spline. *Numerical Algorithms*, 43(1):1017–1398, September 2006.

[5] Y.-S. Chang, K. T. McDonnell, and H. Qin. A new solid subdivision scheme based on box splines. In *SMA '02: Proceedings of the Seventh ACM Symposium on Solid Modeling and Applications*, pages 226–233, New York, NY, USA, 2002. ACM.

[6] Y.-S. Chang and H. Qin. A unified subdivision approach for multi-dimensional non-manifold modeling. *Computer-Aided Design*, 38(7):770–785, 2006.

[7] C. K. Chui, K. Jetter, and J. D. Ward. Cardinal interpolation by multivariate splines. *Mathematics of Computation*, 48(178):711–724, April 1987.

[8] C. K. Chui and M.-J. Lai. Algorithms for generating B-nets and graphically displaying spline surfaces on three- and four-directional meshes. *Computer Aided Geometric Design*, 8(6):479–493, 1991.

[9] J. H. Conway and N. J. A. Sloane. *Sphere Packings, Lattices and Groups*. Springer-Verlag New York, Inc., New York, NY, USA, 3rd edition, 1998.

[10] C. de Boor and K. Höllig. Approximation order from bivariate C^1-cubics: A counterexample. *Proceedings of the American Mathematical Society*, 87(4):649–655, April 1983.

[11] C. de Boor and K. Höllig. Bivariate box splines and smooth pp functions on a three direction mesh. *Journal of Computational and Applied Mathematics*, 9(1):13–28, 1983.

[12] C. de Boor, K. Höllig, and S. Riemenschneider. Bivariate cardinal spline interpolation on a three direction mesh. *Illinois Journal of Mathematics*, 29:533–566, 1985.

[13] C. de Boor, K. Höllig, and S. Riemenschneider. *Box splines*. Springer-Verlag New York, Inc., New York, NY, USA, 1993.

[14] D. E. Dudgeon and R. M. Mersereau. *Multidimensional Digital Signal Processing*. Prentice-Hall, Inc., Englewood Cliffs, NJ, 1984.

[15] A. Entezari. *Optimal Sampling Lattices and Trivariate Box Splines*. PhD thesis, Simon Fraser University, 2007.

[16] A. Entezari, R. Dyer, and T. Möller. Linear and cubic box splines for the body centered cubic lattice. In *VIS '04: Proceedings of the Conference on Visualization '04*, pages 11–18, Washington, DC, USA, 2004. IEEE Computer Society.

[17] A. Entezari, R. Dyer, and T. Möller. From sphere packing to the theory of optimal lattice sampling. In *Mathematics and Visualization*, pages 227–255. Springer Berlin Heidelberg, 2009.

[18] A. Entezari, D. Van De Ville, and T. Möller. Practical box splines for reconstruction on the body centered cubic lattice. *IEEE Trans. Vis. Comput. Graph*, 14(2):313–328, 2008.

[19] P. O. Frederickson. Quasi-interpolation, extrapolation and approximation on the plane. In *Proc. Manitoba Conf. on Numerical Mathematics*, pages 159–176, Winnipeg, Canada, 1971.

[20] H. Freudenthal. Simplizialzerlegungen von beschränkter Flachheit. *Annals of Mathematics*, 43:580–582, 1942.

[21] C. Hamitouche, L. Ibáñez, and C. Roux. Discrete Topology of A_n^* Optimal Sampling Grids. Interest in Image Processing and Visualization. *Journal of Mathematical Imaging and Vision*, 23(3):401–417, November 2005.

[22] K. Jetter and P. G. Binev. Cardinal interpolation with shifted 3-directional box splines. *Proc. Royal Soc. Edinburgh, Sect. A*, 122:205–220, 1992.

[23] R.-Q. Jia. Approximation order from certain spaces of smooth bivariate splines on a three-direction mesh. *Trans. Amer. Math. Soc.*, 295:199–212, 1986.

[24] M. Kim, A. Entezari, and J. Peters. Box spline reconstruction on the face-centered cubic lattice. *IEEE Transactions on Visualization and Computer Graphics*, 14(6):1523–1530, 2008.

[25] H. R. Künsch, E. Agrell, and F. A. Hamprecht. Optimal lattices for sampling. *IEEE Transactions on Information Theory*, 51(2):634–647, 2005.

[26] M.-J. Lai. Fortran subroutines for B-nets of box splines on three- and four-directional meshes. *Numerical Algorithms*, 2(1):33–38, 1992.

[27] A. Levin. Polynomial generation and quasi-interpolation in stationary non-uniform subdivision. *Computer Aided Geometric Design*, 20(1):41–60, 2003.

[28] J. Martinet. *Perfect Lattices in Euclidean Spaces*. Springer-Verlag Berlin Hidelberg, 2003.

[29] T. Meng, B. Smith, A. Entezari, A. E. Kirkpatrick, D. Weiskopf, L. Kalantari, and T. Möller. On visual quality of optimal 3D sampling and reconstruction. In *GI '07: Proceedings of Graphics Interface 2007*, pages 265–272, New York, NY, USA, 2007. ACM.

[30] R. M. Mersereau. The processing of hexagonally sampled two-dimensional signals. *Proceedings of IEEE*, 67(6):930–949, June 1979.

[31] X. Shi and R. Wang. Spline space and its B-splines on an $n + 1$ direction mesh in $\mathbb{R}^n$. *J. Comput. Appl. Math.*, 144(1-2):241–250, 2002.

[32] T. Theußl, T. Möller, and M. E. Gröller. Optimal regular volume sampling. In *VIS '01: Proceedings of the Conference on Visualization '01*, pages 91–98, Washington, DC, USA, 2001. IEEE Computer Society.

[33] D. Van De Ville, T. Blu, M. Unser, W. Philips, I. Lemahieu, and R. V. de Walle. Hex-splines: A novel spline family for hexagonal lattices. *IEEE Transactions on Image Processing*, 13(6):758–772, June 2004.